COMPARATIVE DESIGN AND ANALYSIS OF ON-BOARD CHARGER TOPOLOGIES IN EV CHARGING SYSTEMS FOR OPTIMUM PERFORMANCE

A THESIS SUBMITTED TO THE GRADUATE SCHOOL OF APPLIED SCIENCES OF NEAR EAST UNIVERSITY

By
OLUWAPONMILE DAVID ALAO

In Partial Fulfillment of the Requirements for the Degree of Master of Science in Electrical and Electronics Engineering

NICOSIA, 2017

Oluwaponmile David Alao: COMPARATIVE DESIGN AND ANALYSIS OF ON-BOARD CHARGER TOPOLOGIES IN EV CHARGING SYSTEMS FOR OPTIMUM PERFORMANCE

Approval of Director of Graduate School of Applied Sciences

Prof. Dr. Nadire ÇAVUŞ

We certify this thesis is satisfactory for the award of the degree of Masters of Science in Electrical and Electronics Engineering

Examining Committee in Charge:

Prof.Dr. Mehmet Timur Aydemir	Supervisor, Department of Electrical and Electronics Engineering, NEU
Assist.Prof.Dr. Samet Biricik	Department of Electrical and Electronics Engineering, LAU
Dr. Umar Ozgunalp	Department of Electrical and Electronics Engineering, NEU

I hereby declare that all information in this document has been obtained and presented in accordance with academic rules and ethical conduct. I also declare that, as required by these rules and conduct, I have fully cited and referenced all material and results that are not original to this work.

Name, Last name: Oluwaponmile Alao
Signature:
Date:

ACKNOWLEDGEMENTS

With a sincere heart, I would like to express my deep gratitude and appreciation to my supervisor, Prof. Dr. Mehmet Timur Aydemir. His knowledge, research attitude and ways of thinking are most valuable to me. His able guidance, expertise, patience, and intelligent supervision were essential during my graduate studies at Near East University.

I also acknowledge the Head of the Department of Electrical and Electronic Engineering, Prof. Dr. Senol Bektas, for provision of the academic platform where student can acquire a sound knowledge in the field of Electrical and Electronic Engineering.

I appreciate my parents Rev. and Mrs. James M. Alao. They have inspired me throughout my life and have taught me the best lessons of life in love. My appreciation also goes to my siblings for their love, care, support and the understanding shown to me during the course of my graduate program.

Finally, I would like to thank the Department of Electrical and Electronics Engineering for supporting me during my years of study at Near East University.

To my parents…

ABSTRACT

There is no ambiguity in the fact that the usage of plug-in electric vehicle (PEV) is now in the increase due to the numerous advantages it possesses over the conventional internal combustion engine (ICE) vehicles which consume more fuel and also raise concerns globally over global warming and climate changes.

This Master's Thesis is committed to the design of a PEV battery charger with two stages and a comparative analysis of the dc-dc resonant converter stage based on the performance of half-bridge LLC and half-bridge LLC-LC dc-dc converter topologies from the simulation result. This has a significant overall bearing on the operation and efficiency of the hybrid electric vehicle on-board charger.

Two different EV chargers of 2.2kw design are presented and investigated with the difference coming mainly from the second (dc-dc) stage topology which consists of LLC resonant converter and the other an improved LLC topology.

The theoretical mathematical calculations for the converters components are performed while the circuits simulations are carried out using MATLAB Simulink. At the resonant converter stage, the circuit is modeled so that its operation is at resonance frequency in order to have very high efficiency and a small turnoff current for the switches so as to decrease switching losses. The whole procedure is presented in the report.

Keywords**:** Battery charger; electric vehicle; boost converter; resonant converters;

zero voltage switching.

ÖZET

Elektrikli araçların (EV), yakıt tüketimi daha yüksek olan ve küresel kirlenme ve iklim değişikliği konularında olumsuz etkileri bulunan geleneksel içten yanmalı motorlu araçlara göre üstünlükler içerdiği ve bu nedenle kullanımlarının sürekli olarak artış gösterdiği konusunda bir tereddüt bulunmamaktadır.

Bu tez çalışmasında PEV araçlarda kullanılan iki aşamalı batarya şarj devreleri ele alınmıştır. Yarı köprü LLC ve yarı köprü LLC-LC rezonanslı DA-DA dönüştürücü topolojilerinin karşılaştırmalı analizi benzetim aracılığıyla gerçekleştirilmiştir. Bu devreler hibrit elektrikli araçların araç üstü şarj devrelerinin çalışması ve verimi açısından önemli kazanımlara sahiptir.

İncelenen ve tasarımı yapılan her iki devrenin gücü de 2.2 kW olup, devreler arasındaki fark sekonder tarafında kullanılan DA-DA dönüştürücü yapısındadır. Bir devrenin sekonderinde LLC rezonanslı dönüştürücü, diğerinde ise geliştirilmiş bir LLC devresi bulunmaktadır.

Dönüştürücüler analitik olarak analiz edilmiş ve performansları MATLAB yazılımında benzetim yolu ile incelenmiştir. Rezonans dönüştürücü katında devre, verimi yüksek tutmak amacıyla anahtarlama kayıplarını düşürecek tıkama akımları elde edebilmek için, rezonans frekansında çalışacak biçimde tasarlanmıştır. Tüm tasarım süreci raporda verilmektedir.

Anahtar Kelimeler: Batarya şarj devresi; Elektrikli araçlar; Boost dönüştürücü; Rezonans dönüştürücüler; Sıfır gerilim anahtarlama

TABLE OF CONTENTS

CHAPTER 3: SET-UP DESCRIPTION

CHAPTER 4: RESULTS AND DISCUSSION

LIST OF FIGURES

LIST OF TABLES

CHAPTER 1

INTRODUCTION

1.1 Background

Increased attention over environmental impact has resulted into more research been geared towards more eco-friendly technologies in every relevant scientific field and sector. In the case of automotive industry, the reduction of heavy dependence on fossil fuels is a major concern apart from the pollution and climate change factors. One of the most reliable alternatives is found in the advancement of electric vehicles (EVs) technology.

The new development has made car manufacturers to incorporate more of electric components and systems in conventional ones or even replacing it with wholly electrical ones. This lead to the development of what is called hybrid electric vehicles (HEVs) which was devised over a century ago. In recent years, there has been growing research into electric vehicles at an advanced rate. Several experiments and relevant improvements have been carried out with many feasible models built.

The battery has a vital part in this electric vehicles (EVs) build up. An electrical vehicle which is driven by electricity, as different from conventional ones which still represent the majority on the roads and are leading consumers of fossil fuels, has its electricity produced either externally from the EV itself and are collected in the battery or internally through fuel cells. A battery transforms chemical energy straight into electrical energy. It has the capacity to store chemical energy. Batteries are therefore highly desirable for vehicular usage. The traction battery is especially utilized by electric vehicle producers. Examples of traction battery are Nickel and Cadmium, Sodium and Nickel Chloride, Lead Acid type, and a few others. There exists certain standards that are needed of batteries when it comes to energy density, safety, and life cycle so as to be practically applicable in EVs and PHEVs. They should be able to store large amount of energy and possess a long life cycle. This will make it possible for the vehicle to be able to cover large distance before the battery is almost completely discharged and need to be recharged.

This leads to battery charging and EV battery chargers. Lithium-ion (Li-ion) is widely used in EVs due to its superiority in the supply of very high discharge power needed for rapid acceleration and also high energy density. These makes it operate at higher efficiency and also its lower weight makes it the most used type in the automotive industry application (Wang, Dusmez, & Khaligh, 2014). Figure 1.1 below depicts charging profile for Lithium-ion battery cell (Dearborn, 2005). The general charging process utilized for a Lithium-ion battery comprises of two-stage process namely: constant current or CC charging and constant voltage or CV charging. Starting with constant current charging, the charging current is kept at the same constant value while the battery voltage rises from its former level to a higher value. After this, the process switches to common voltage charging, where charging voltage remains constant at the specific final value and the current reduces to the lowest point, then the charging ends (Kisacikoglu, Ozpineci, & Tolbert, 2011).

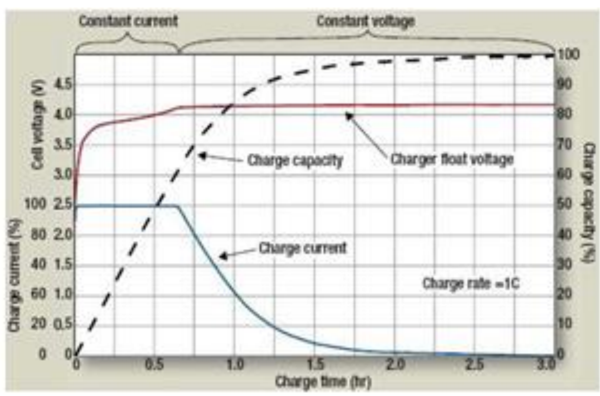

Fig.1.1: Lithium-Ion Cell Charging Profile

In recent years, several EV charger topologies with their various advantages and disadvantages and also compromises have been proposed and built through different researches carried out. EV chargers can therefore be classified into different sections considering their configurations and topologies which are found on particular general design and areas of application. The table below (Kisacikoglu et al., 2011)gives five methods of charger classification.

Table1.1: Classification of EV battery charger

Classification type	Options
Topology	Dedicated, Integrated
Location	On-board, Off-board
Connection type	Conductive, Inductive, Mechanical
Electrical waveform	AC, DC
Direction of power flow	Unidirectional, Bidirectional
Power level	Level1, Level2, Level3

Based on circuit topology classification, it can be a dedicated circuit which functions mainly to charge the battery. It can also function as an integral/integrated charger. An example of this is the traction inverter drive which is also able to serve as the charger during the EV motionless state and plugging to grid for charging. The number two in the table is based on charger location. It is either on-board which makes the EV readily accessible to be charged, or off-board. For an off-board topology, the battery is not integrated in the electric vehicle. On-board chargers are able to supply energy storage system applications like voltage regulation and reactive power compensation without connecting the battery to the grid. This helps in preserving the battery lifetime (Kisacikoglu, Ozpineci, & Tolbert, 2013)

Fig.2 shows the make-up of an electric vehicle battery charger. It is a two-stage structure. The first, being ac-dc converter and the second is a dc-dc converter stage.

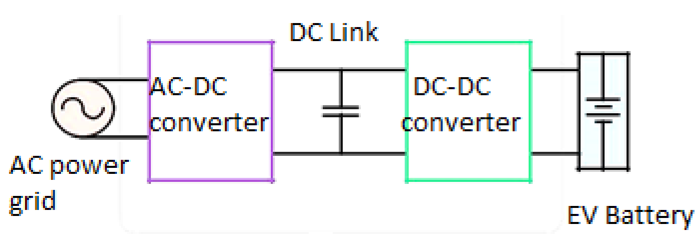

Fig.1.2: Typical Power Architecture of an EV Battery Charger

Topology used in this project has interaction with the grid through the ac-ad converter stage as shown in Fig. 1.2. As will be shown in the model development in later chapters, there is the presence of sizable filter capacitor (C_f) in rectifier diodes output at the first stage. This results in the line current loosing its sinusoidal form. At every cycle, C_f is charged at (or close to) alternating voltage peak, that is Peak Vac and this gives line input current both positive and negative pulses which contain harmonic distortion (Kazimierczuk, 2012). This ac-dc part therefore will also act as a power factor correction stage by monitoring the THD at line input current through ensuring that it is in phase with the voltage so that PF is near unity and, in turn, have the expected voltage output of the ac-dc converter regulated at dc-link capacitor. Then comes the second stage of the EV charger model which balances the charging current for common current charging and the charging voltage for the EV battery common voltage charging. The research makes use of the ZVS topologies of resonant converters at the second stage due to their inherent advantages of soft-switching and therefore less switching losses and increase efficiency of the EV charger.

1.2 Literature Review

The development of electric vehicles began over a century ago around 1834. The electric vehicle powered by a battery was developed by Thomas Davenport (Chau & Wong, 2002), this was even before the creation of ICE which is makes use of diesel and gasoline fuel. But its development was halted because they were not very convenient at the time due to their weight and also took very long time to recharge. And again, by the year 1911, they were more costly than ICE.

Due to concerns over depletion of fossil fuels and pollution factor, attention has been shifted back to development of vehicles driven by alternative fuels. Nowadays, millions of electric vehicles ply the roads and car manufacturers are improving on the technology for optimum efficiency and cost reduction. This has called for constant research and work on one of the very important components of the EV which is the battery charger.

In recent years, several charger topologies have been researched and proposed. Recently, Kisacikoglu et al proposed a double stage EV charger which consists of a full-bridge ac-dc boost converter with half-bridge dc-dc converter. It was proposed with emphasis on reactive power support (Kisacikoglu, Kesler, & Tolbert, 2015).

In another study, Bolte et al designed and proposed a 2KW isolated on-board dc-dc converter for power distribution systems in electric vehicles. In the work, a hard-switching buck converter is designed in the first stage for voltage control while a SRC for isolation transformer is designed for second stage (Bolte, Froehleke, & Boecker, 2016).

Several researches have been carried out on mainly investigating EV chargers with bi-directional topology for PEVs (Yilmaz & Krein, 2013). Other studies have surveyed different EV chargers, both single-phase and three-phase ac–dc converter topologies which are appropriate for vehicle to grid applications (Erb, Onar, & Khaligh, 2010).

There has also been many work presented on different topologies of resonant converters which also find applications in EV. R. Severns proposed different topologies for resonant converters (Severns, 1992). In his work, Rani et al also analyzed the design of full bridge SPRC for battery chargers (Rani, Samantaray, & Dash, 2013). And many LLC resonant converters have been designed at the dc-dc stage for electric vehicle battery chargers.

It should be noted that most designs and implementations in the articles and researches undergo different scientific investigation and evaluation of several topologies while a few connect their survey by way of comparative analysis of topologies so as to emphasis the different applications befitting for each topology presented. The analysis in this paper aim to tread on a similar path by undergoing a comparative analysis of two proposed EV charger with one being an improvement on the second stage topology of the previous and looking at the strength and weaknesses of both topologies.

1.3 Goals and Objectives

The objective of the thesis is to design a model of electric vehicle on-board charger which can provide the needed optimum performance with less losses in the system. This will be achieved through the comparative analysis of different design of converter topologies. In order to achieve this, the following objectives will be pursued:

1. The design and simulation of the charging system's ac-dc converter (boost) making use of the proposed boost converter.

2. The design and simulation of the systems ad-dc converter proposing resonant converters with soft switching capability and of different topologies at this stage.

3. Compare and discuss the results of the different EV charger system topologies in terms of their output performance during simulation.

The tasks to be performed in this thesis work can be divided into the following sub-sections, and each will be properly analysed:

• Simulation of the developed models

• Waveforms attainment

• Analysis & comparison

• Conclusion and future suggestions

All simulations are performed making use of MATLAB/SIMULINK environment.

1.4 Method

• Study several literature and documentations that are related to the project

• Get familiar with MATLAB/SIMULINK and build up different converter topologies in the software

• Analyze the performance of the different models and spell out the weaknesses of anyone with other areas where they can find save and accurate application.

• Compare the different resonant converter topologies in the second stage of the EV charger, and verify the simulated performance through studying of relevant waveforms

• Determine and quantify important parameters which assist in proper understanding and accurate evaluation of the proposed models, such as the efficiency, losses etc.

• Analyze and verify the obtained results, and if necessary, suggest possible improvements.

1.5 Thesis Outline

Along with the Introduction, the project is arranged over five chapters.

Chapter 2 gives an introduction to the different converter types, their categorization and analysis. Chapter 3 presents the mathematical modeling of the boost and resonant converters used in the proposed model(s) of this thesis. In Chapter 4, the simulation results are presented. And chapter 5 provides conclusions and further or future work suggestions are made.

CHAPTER 2

THEORY OVERVIEW

2.1 Basic Converter Topologies

There exists different converter topologies and all these have been made use in different areas of applications both individually and/ or in combination. In order to obtain an accurate knowledge of how converters work and their functions in numerous applications and also their performance, their basic explanation, rudimentary and central importance are included in this chapter. The three primary forms at the dc-dc level, the buck converter, boost converter, buck-boost converters with a few more and resonant converters will be explained in this chapter as they are vital to the EV charger models proposed in this thesis. These are primarily used in battery-powered applications and also in devices which need different voltage levels. There are many topologies for DC/DC conversion, such as buck, boost, buck-boost, forward, cuk, flyback, push-pull converters etc. Additionally, usually a distinction is made between isolated and non-isolated converters. In many applications multiple outputs are required, safety standards need to be met and impedance matching must be provided, therefore output isolation may be required to be implemented. Since this project is dealing with an application which is in electric vehicles, several different topologies are available for usage. However, this project will concentrate on the dc-dc converters, for at the ac-dc stage of the proposed EV charger, the model is designed with a double section which makes use of rectifier diodes, which converts the ac signal from the grid into dc, and then the boost converter. This chapter will therefore give an overview of buck, boost, buck-boost, cuk, flyback, forward, Isolated and non-isolated and resonant converters. These types are regularly employed in EV charger models.

2.1.1 Buck converter

A buck converter which is also called step-down converter gives an average output voltage that is less than input dc-voltage. A buck converter circuit is depicted in Figure 2.1 below.

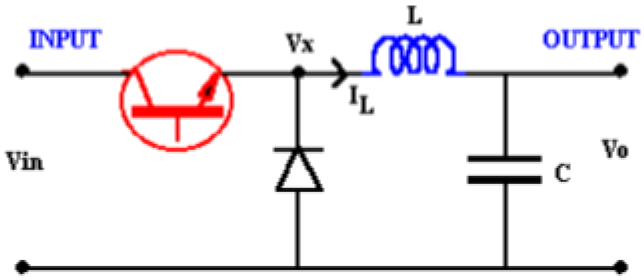

Fig. 2.1: Step-down Converter

From Fig. 2.1 above, the output voltage is the same as voltage input (Vin) when switch is in ON position during the interval Ton $\geq t \geq 0$. Vin tends to increase the inductor current. During the switch OFF position, the current continues its passage through the inductor but the flow is now through the diode.

At t = 0, switch is now turned on, and off at t = Ton.

The switching device which is a thyristor here switches the input voltage to the load when been triggered at specific instants. The diode present acts as a free wheeling through which the load current passes when the thyristor is turned OFF. The absence of such diode may result in the damage of the switching device as result of high induced EMF in the inductance.

In order to analyze the voltages in a buck converter circuit, the inductor current variation over one cycle is taken into consideration. Using the equation below:

$$V_x - V_0 = L\frac{di}{dt} \tag{2.0}$$

The current change yields:

$$di = \int_{ON}(V_x - V_0)dt + \int_{OFF}(V_x - V_0)dt \tag{2.1}$$

During steady state operation there exists no variation in the current at both the beginning and end of a period T. in order to obtain a simple relation of the voltages, take voltage drop across both the diode and transistor to be zero in the ON position and a perfect switch change assumption is observed. Therefore, at ON time Vx = Vin and in the OFF time Vx = 0. Therefore:

$$0 = di = \int_{0}^{t_{on}} (V_{in} - V_o)dt + \int_{t_{on}}^{t_{on}+t_{off}} (-V_o)dt \qquad (2.3)$$

Simplifying the above gives

$$(V_{in} - V_o)t_{on} - V_o\, t_{off} = 0 \qquad (2.4)$$

That is:

$$\frac{V_o}{V_{in}} = \frac{t_{on}}{T} \qquad (2.5)$$

Therefore:

$$D = \frac{t_{on}}{T} = \frac{V_o}{V_{in}} \qquad (2.6)$$

Where ‘D’ represents the duty ratio of the buck converter.

2.1.2 Boost converter

A boost converter which is also called step-up converter gives a voltage output that is greater than the voltage input. A step-up converter circuit is depicted in Fig. 2.1 below.

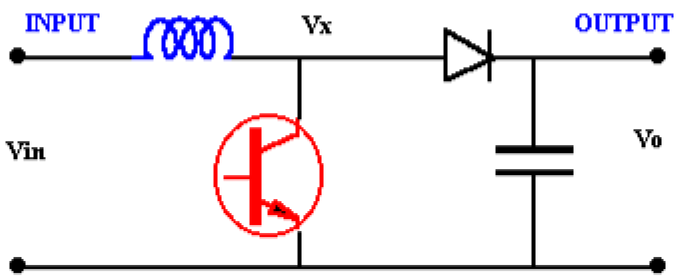

Fig. 2.2: Step-up Converter

In similar manner as the buck converter, a diode is in series with the load which allows the passage of the load current when thyristor is turned OFF.

During the ON state of the transistor, Vx =Vin, and when it is OFF, the inductor current passes through the diode resulting into: Vx =Vo. This means the load gets the voltage from input and also from inductor, resulting in the voltage at the converter output to be more than that of the input. In this study it is supposed that the inductor current keeps flowing (continuous conduction). The average of the inductor voltage have to be zero for the average current to continue in steady state. Therefore:

$$V_{in} t_{on} + (V_{in} - V_o) t_{off} = 0 \tag{2.7}$$

This is rearranged and simplified as:

$$\frac{V_o}{V_{in}} = \frac{T}{t_{off}} = \frac{1}{(1-D)} \tag{2.8}$$

Where 'D' is the duty ratio for the boost converter. Voltage output can be varied through the variation of the duty ratio till the load has the expected voltage.

2.1.3 Buck-boost converter

A buck-boost converter can be used in both step-down and step-up operation through the continuous adjustment of the duty cycle. The circuit for this converter is shown in Fig. 2.3. it has only a single switching device, which is one thyristor. Alongside an inductor and diode, another capacitor is connected in parallel with the circuit.

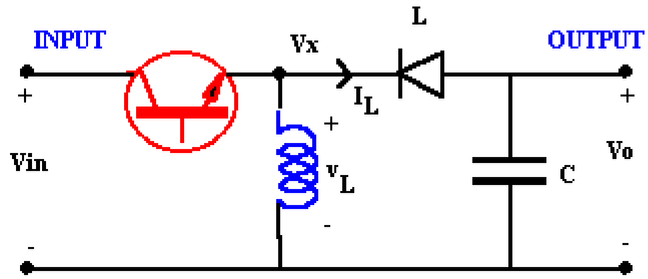

Fig. 2.3: Buck-Boost Converter

When switch is turned ON, the supply current passes to the inductor through the thyristor, thereby inducing the inductor voltage.

When the switch is turned OFF, the current in the inductor to reduces with the induced emf reversing polarity. The converter output voltage remains constant as a capacitor is connected across the load.

Through the variation of the duty ratio within the range $0 \geq k > 0.5$, the voltage output is lesser than its input, and a buck converter is thereby realized.

While the output voltage will be more than the input if the duty ratio falls within the range of $0.5 > K \geq 1$, therefore giving rise to a boost converter.

2.1.4 Cuk converter

The three converters discussed above all convey energy between input and output making use of the inductor and their circuits are analyzed in reference to voltage balance across the inductor. In the case of CUK converter, it utilizes a capacitor to convey energy and it is analyzed in reference to current balance of the capacitor. The circuit of a CUK converter is as depicted in the figure below.

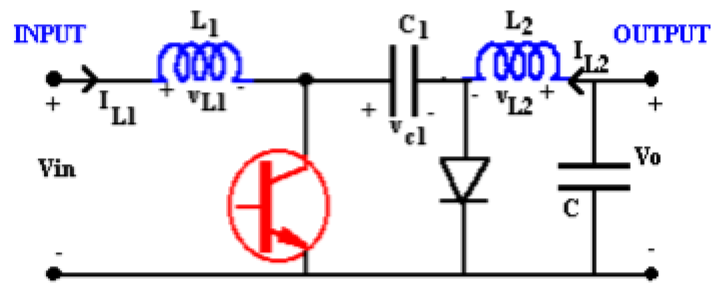

Fig. 2.4: CUK Converter

CUK converter has to its merit that there is creation of a smooth current at the two converter sides by the input and output inductors, while both the buck and boost converters alongside buck-boost, all are with at least one side with pulsed current.

2.2 Non-Isolated and Isolated Converters

Non-isolated converters are most suitable where there is the need for the voltage to be stepped up or down by a comparatively modest ratio (< 4:1). Also, when there exists no technical issue with the absence of dielectric isolation between the source and the load output end, non- isolated converters are commonly utilized. The four basic types of converter that belong to the non-isolated division have been discussed above. It should be recalled that the buck converter steps down the voltage and the boost converter steps the voltage up. The buck-boost and Cuk converters are able to function as either step-down or step-up.

Isolated converters are deemed important in applications where the output must be totally isolated from the input. It is also desired in order to meet safety standards and also provide impedance matching. A high frequency transformer is generally used for the isolation in these set of converters. Examples of converters in this division are Fly-back, Forward, Half-Bridge, and Full-Bridge DC/DC converters (Garcia, Flores, Oliver, Cobos, & de la Pena, 2005). These converters are able to operate as bi-directional converters. Also, the ratio of voltage step-up or step-down is high.

2.2.1 Flyback converter

A flyback converter represents a development on the Buck-Boost converter. Fig. 2.5 below show a flyback converter in which the inductor is replaced by a transformer. The flyback converter works through the storage of energy in the magnetization of the transformer core during the ON phase and having it released unto the output during the OFF phase. In order for stored energy increment, a core with gap is usually utilized.

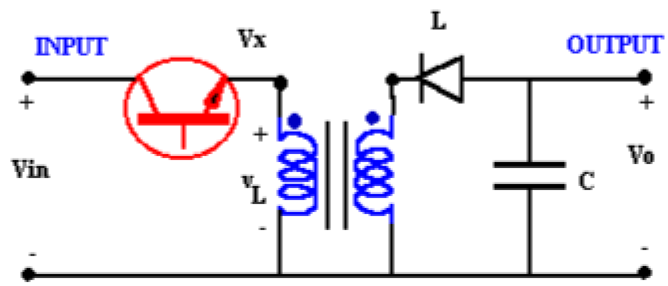

Fig. 2.5: Flyback Converter

2.2.2 Forward converter

The main idea behind forward converter is the conversion of input AC voltage by the ideal transformer to an isolated secondary output voltage. As shown in Fig. 2.6, during transistor ON state, the input voltage appears across the primary and produces:

$$V_x = \frac{N_1}{N_2} V_{in} \tag{2.9}$$

The function of the first diode at the output end after the transformer is to make certain that the voltages applied to the output circuit are positive. The second diode maintains a circulating path for the current through the inductor if the transformer voltage is negative or zero.

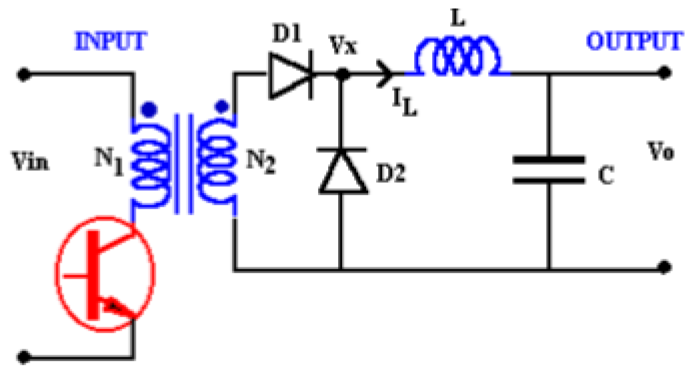

Fig. 2.6: Forward Converter

2.3 Basic Resonant Converters

In the 1980's, the resonant converters were thoroughly studied (Liu, Oruganti, & Lee, 1985). These set of converters are able to actualize very low switching loss therefore facilitate the operation of resonant topologies at high switching frequency. The top most familiar resonant topologies are the Series Resonant Converter (SRC), Parallel Resonant Converter (PRC) and Series Parallel Resonant Converter (SPRC). These topologies and other popular ones are investigated and properly analysed in this section.

2.3.1 Series resonant converter

The resonant tank of a SRC comprises of a resonant inductor Lr and a resonant capacitor Cr which are connected in series. The resonant tank itself is connected in series with the rectifier-load network. Fig. 2.7(a) shows the circuit diagram of a half bridge SRC. From this arrangement, the resonant tank forms a voltage divider with the load. Any alteration in the frequency of the driving voltage automatically changes the resonant tank impedance. The voltage at the input is divided between the impedance and reflected load (Yang, Lee, & Jovanovic, 1992). The DC gain of series resonant converter is generally less than unity. Fig. 2.7(b) depicts the gain curve of series resonant converter. There is a sizable load impedance during light-load mode as compared to the resonant network impedance. This is because all input voltage is burdened on the load. This results into difficulty in the regulation of the output voltage at light load. From theory, an infinite frequency is required for the regulation of the output voltage at no load condition.

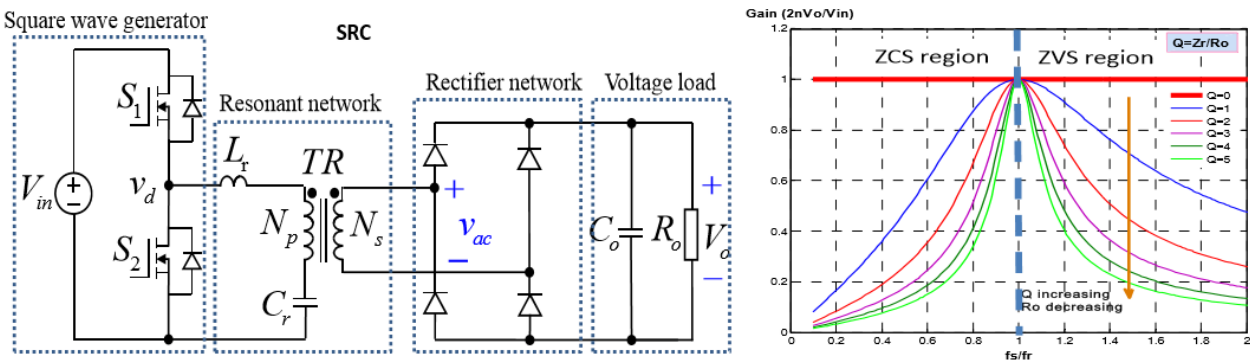

(a) SRC Circuit

(b) SRC Gain Curves

Figure.2.7: Series Resonant Converter(Wan, 2012)

The converter operates under zero current switching (ZCS) condition for Fsw < Fo. For Fsw > Fo , the converter functions under zero voltage switching (ZVS) condition. ZVS is desired for MOSFET switch. It should be noticed from operating region that at light load, Fsw is required to be very high to ensure the regulation of the output voltage. This poses a big demerit for series resonant converters. In order to therefore ensure output voltage regulation at light load, inclusion of other control technic is vital. The primary disadvantage of series resonant converters which limit their areas of application is therefore light load regulation

2.3.2 Parallel resonant converter

For a parallel resonant converter (PRC), the load is in parallel with the resonant capacitor. The primary side of the transformer is a capacitor, this therefore necessitates the addition of an inductor at the secondary side for impedance matching. Figure 2.8 (a) shows the circuit diagram of a half bridge PRC.

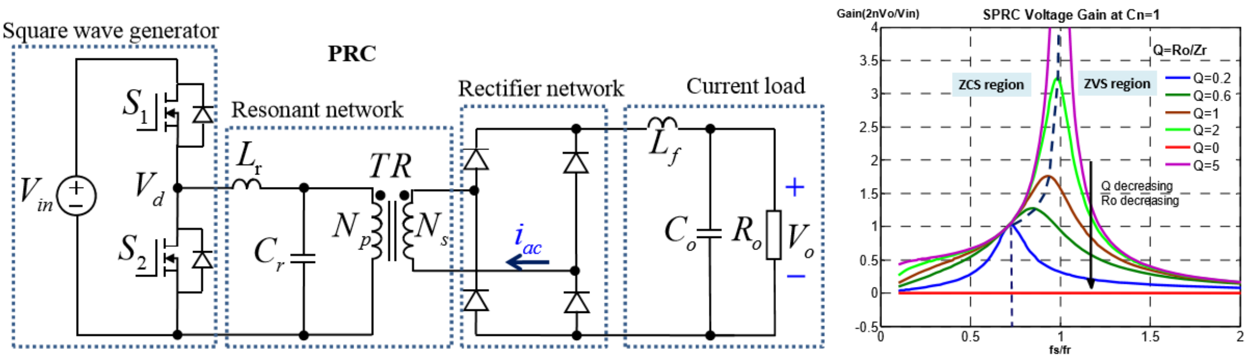

(a) PRC Circuit (b) PRC Gain Curves

Fig. 2.8: Half-bridge Parallel Resonant Converter(Wan, 2012)

Fig. 2.8(b) shows the gain curve of parallel resonant converter. Similar to that of series resonant converter, the operating region is configured on the RHS of Fo in order to achieve ZVS. In comparison with the series resonant converter, it has a smaller operating region is much smaller due to a more steep curve. The frequency does not need a large variation to maintain output voltage regulation at light-load. This is an obvious merit over SRC (Kang, Upadhyay, & Stephens, 1991). However, at when the input voltage is high, the converter operates at a high frequency far from Fo. And from MOSFET current, the turn off current is very small for lower input. Therefore the circulating energy is very high in comparison with SRC, even at light-load. The primary disadvantages of parallel resonant converters which limit their areas of application are therefore: high circulating energy and a high turn-off current for high input voltage condition.

2.3.3 Series parallel resonant converter

The resonant tank of a PSRC comprises of a resonant inductor Lr, a resonant series capacitor Csr, and a parallel resonant capacitor Cpr. SPRC resonant tank is a combination of SRC and PRC. Just like PRC, there is the addition of an output filter inductor at the secondary side for impedance matching. Fig. 2.9 (a) shows the circuit diagram of a half bridge SPRC. A series parallel resonant converter get together the good attributes of SRC and PRC. It has a relatively small circulating energy in comparison with PRC due to series connection of the load with Lr and Csr series tank . SPRC is also able perform output voltage regulation at no load due to presence of the parallel capacitor Cpr.

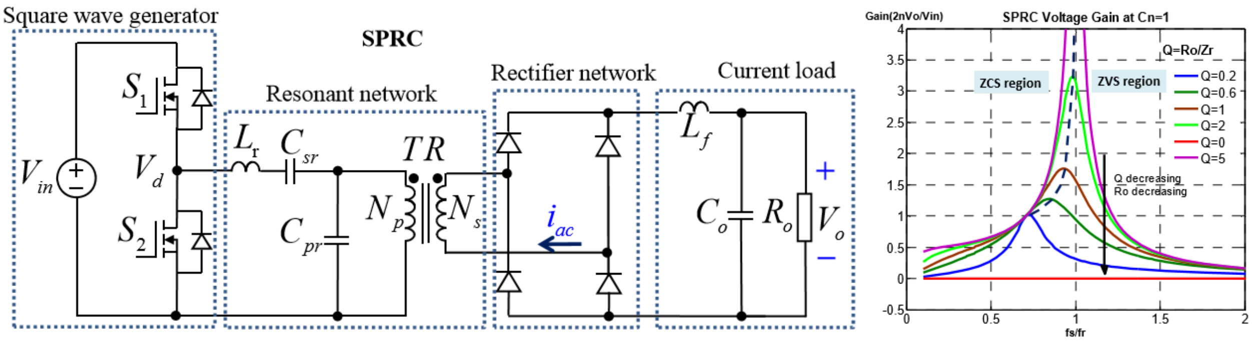

(a) SPRC Circuit (b) SPRC Gain Curves

Fig. 2.9: Series Parallel Resonant Converter(Wan, 2012)

Fig. 2.9(b) depicts the gain curve of SPRC. Similar to that of series resonant converter and parallel resonant converter, the operating region is configured on the RHS of Fo in order to achieve ZVS. It should be noticed from operating region that SPRC close switching frequency varies with change in load in comparison with SRC. It has a much lower input current when compared with PRC and just a little higher than that of SRC. Therefore SPRC has a reduced circulating energy in comparison with PRC (Bhat, 1993). SPRC operates at higher frequency far from Fo at high input voltage, just like SRC and PRC. MOSFET turn-off current and circulating energy get higher at high input voltage, just as in PRC and SRC. A series parallel resonant converter therefore gets together the good attributes of SRC and PRC. That is, a lower circulating energy and relatively lower sensitivity to change in load. However, for wide input applications, switching loss and conduction loss gets higher at as the voltage input increases. This therefore makes SPRC not too suitable for designs with wide voltage input range.

2.3.4 LLC resonant converter

The three resonant converter topologies identified in the previous sections all are not suitable for wide input range design and therefore cannot be optimized at high input voltage. Switching loss and high conduction loss will become the penalty when being utilized for wide input range. Therefore, the most efficient method is for a resonant tank to operate at its resonant frequency. This is also applicable to PRC and SRC. SPRC has two resonant frequencies, but operating at its upper resonant frequency is generally more efficient.

In order to actualize ZVS, the converter must not operate on positive slope of the dc curve. Therefore SPRC is unable to be optimized for wide voltage input. It is similar for PRC and SRC. That is, it will function at Fsw which is far from fo at large voltage input (Tv & Mosfets, 2007). Therefore, a resonant converter is able to have high efficiency at resonant frequency. An LLC resonant converter can be designed as shown in Fig. 2.10 to operate at resonant frequency in order to have a very high efficiency. There are two resonant frequencies in LLC resonant converters. Lsr and Cr decide the higher resonant frequency while Cr and the series inductance of Lpr and Lsr decide the lower Fo The upper resonant frequency falls at the zero voltage switching region, LLC converters can therefore be modeled to function around the resonant frequency.

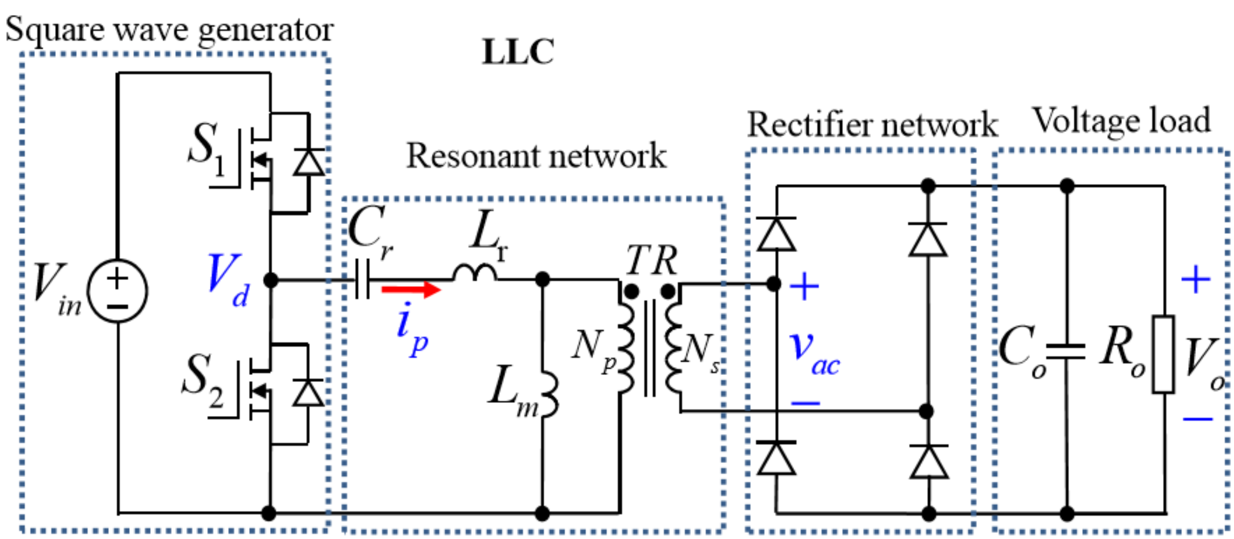

Fig. 2.10: Half-Bridge LLC Circuit (Tv & Mosfets, 2007).

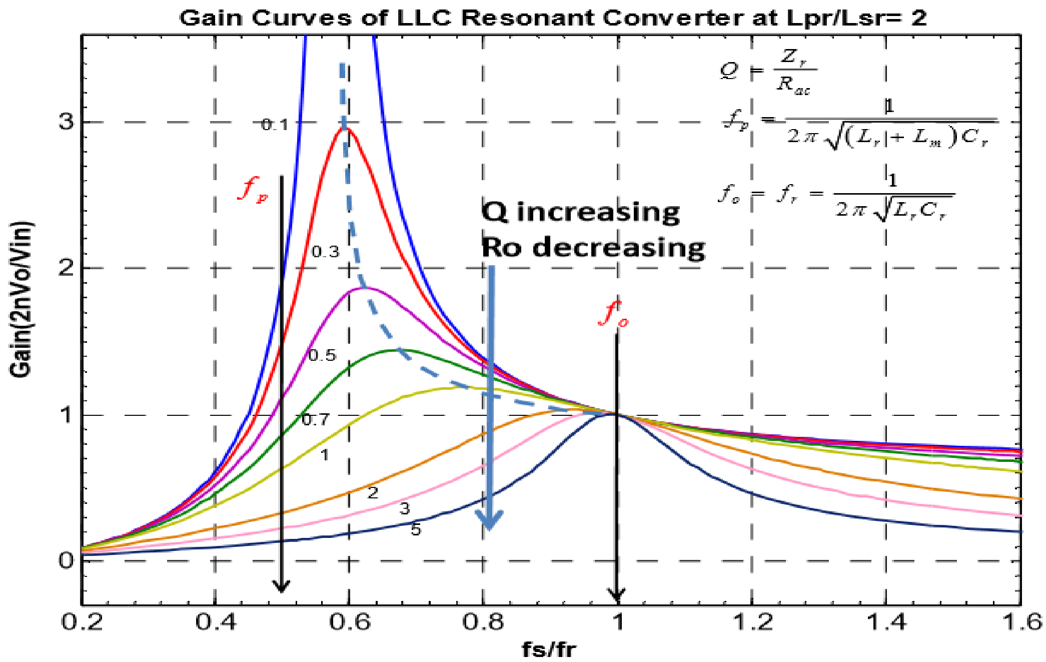

Fig. 2.11: LLC Resonant Converter Gain Curves (Tv & Mosfets, 2007).

2.4 EV Battery Charger Topology Selection

The basic converters overview for the many different topologies applicable in power electronic systems and their basic block diagrams have been looked into under the previous sections. In this research work which comprises of two stages, different topologies can be considered for both stages. Also, several researches and papers have designed different combinations for both stages. In this work, for the ac-dc stage, the boost converter is considered. Since the ac voltage has to be converted unto its equivalent dc magnitude, the ac-dc boost converter consists of rectifier section made up of four rectifier diodes prior to the boost circuit.

Also at the resonant converter stage, many topologies can be examined as possibilities as several researches have proved. Among them the most suitable one chosen for this research work is a soft-switched half-bridge resonant converter which is also zero-voltage switched. These converters are able to attain very high efficiency and excellent device utilization as the theoretical analysis also reveals.

The selection at the dc-dc stage take the application into consideration specifically the power level and the battery voltage. This thesis designs EV battery chargers of 2.2KW. It is reasonable that a relatively high output voltage is needed. Moreover, the battery voltage level used in PEVs generally varies between 200 and 390V (Kisacikoglu, Ozpineci, & Tolbert, 2010). Also, the EV battery charger model falls under level 2, as the AC voltage used is 240Vac and it is designed for 2.2KW output (that is above 2KW) (Kisacikoglu et al., 2010).

The capital cost for implementation of any designed EV charger should also be of primary concern. And thus care is taken that the combination of the converters chosen for both stages does not result into a voluminous design with bulky components.

This thesis presents the combination of both boost and LLC resonant converters for both stages of the EV battery charger, with the LLC resonant converter ensuring zero voltage switching under any load conditions. Therefore, the suitability of the designed EV battery charger for optimum performance is ensured from the utilized converter topologies which favor applications with high efficiency and high power density.

2.5 Zero Voltage Switching

Resonant circuits are usually made use of to shape the voltage and current of switches so as to give rise to zero-voltage or zero-current switching. These methods have been improved upon making use of the principle of resonant switch to confront switching losses in power-electronic devices and also to check electromagnetic interference (EMI) present, as a result of high di/dt and dv/dt occasioned by switch-mode operation. The zero-voltage-switching is able to decrease the total switching losses by over half, while zero-current-switching decreases the switching losses by about a quarter (25%) in comparison with hard switching.

Zero voltage switching topology comes into effect when the switch turns on and off at zero voltage. ZVS method removes switching loss and di/dt disturbances as a result of MOSFET’s junction capacitances discharging and it also ensures that converters function at high switching frequencies. In order to achieve ZVS, there must be enough dead-time during which the switches are off and duty cycle loss occurs due to the absence of power been delivered to the load. Figure2.11 below depicts how adequate dead-time can be obtain in order to effect zero voltage switching.

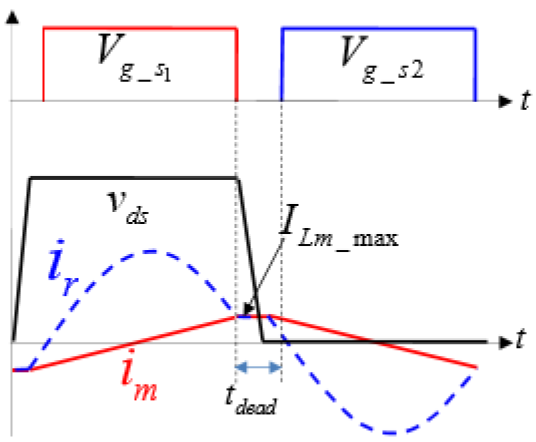

(a) Curves

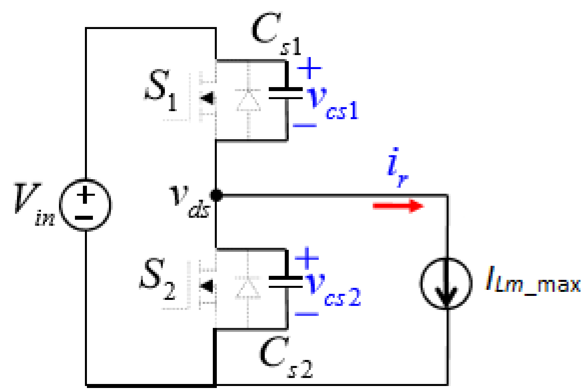

(b) Circuit

Fig.2.12: Dead-Time Requirement for ZVS

From Fig. 2.11, C_{S1} and C_{S2} represents the junction capacitances of the two switches respectively. Also;

$$I_{Lm\_\max} = \frac{nV_o}{L_m} \cdot \frac{T}{4} \tag{2.10}$$

Thus, for the realization of zero voltage switching the turn-off current must be capable of discharging and charging the junction capacitors during the dead-time interval. It demands that the turn-off current must be smaller than the magnetizing inductor's maximum current. Therefore;

$$C_{s1}\frac{du_{cs1}}{dt} + C_{s2}\frac{du_{cs2}}{dt} = i_r \le I_{Lm\_\max} = \frac{nV_o}{L_m} \cdot \frac{T}{4} \tag{2.11}$$

Therefore, the dead-time must be able to satisfy that:

$$t_{dead} \geq 8L_m \left(C_{s1} + C_{s1}\right) f_s \tag{2.12}$$

CHAPTER 3

SET-UP DESCRIPTION

3.1 Proposed EV Battery Charger

This chapter discusses the design of the proposed charger system developed for this study. It analysis the main model proposed which includes the boost converter for the first stage of the charger system and the LLC resonant converter for the second stage.

It also investigates other improved and/ or possible resonant topologies for the second stage. This serves as the main comparison apparatus for this thesis, which studies the output performance of each.

The result analysis and discussion are done in Chapter 4. MATLAB/Simulink are used for the design of the EV battery charger model.

3.2 Model I

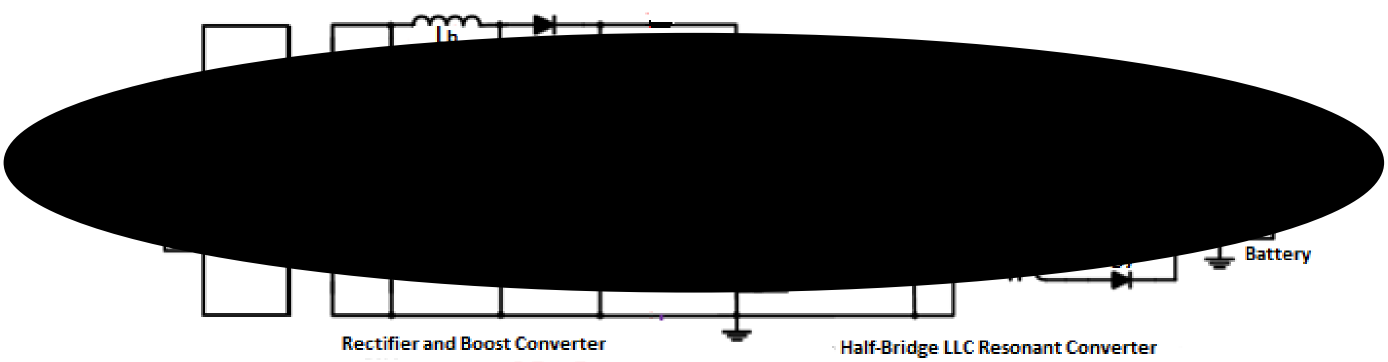

Fig.3.1: Schematic Diagram of the Designed EV Charger

The Fig. 3.1 dpicts the circuit diagram of the designed two stage EV battery charger. The first consists of the rectifier and boost converter and the second consists of LLC resonant converter. Calculations for the design of both stages are shown in the subsequent sub-sections.

3.2.1 The design of boost converter

At the first stage, line current and voltage is rectified from the diode rectifier. The rectifier is followed by the boost converter. EMI filter reduces the ripples found in thecurrent input as a result of hysteresis current control. The rectifier-boost converter stage therefore converts the grid ac-voltage to its regulated DC equivalent at DC-link capacitor and it also decreases total harmonic distortion ofcurrent input so as to give a power factor of one.

After power factor correction in the first stage, the source, that is V_s and I_s, is taken to be sinusoidal. Therefore for the gate signal of S_b, the on-time duty cycle d(t) is given as by (Kazimierczuk, 2008):

$$d(t) = 1 - \frac{|V_s|}{V_{dc}} = 1 - \frac{V_p\,|\sin\omega t|}{V_{dc}} \tag{3.1}$$

Where / V_s/ represents the rectifier output voltage and

V_p is the voltage peak value and

V_{dc} represents the dc-link coltage.

At the ON state of switch S_b , current passing through the inductor has a linear increment and flows through S_b .During the ON state of S_b, the peak value of the current through the inductor (I_{LP}) which passes through the diode is given by:

$$I_D = [1 - d(t)]I_L = \frac{V_p\,I_{LP}}{V_{dc}}\sin^2\omega t \tag{3.2}$$

Therefore;

$$I_D = \frac{V_p\,I_{LP}}{2V_{dc}} - \frac{V_p\,I_{LP}}{2V_{dc}}\cos 2\omega t = I_{b0} + I_{bc} \tag{3.3}$$

Where:

$$I_{bc} = -I_{b0}\cos 2\omega t \tag{3.4}$$

The current at the output of the boost,I_{b0}, is

$$I_{b0} = \frac{V_p I_{LP}}{2V_{dc}} \tag{3.5}$$

This shows that the diode current dc component is equal to the current through the output.The second harmonics of this current passes through the dc-link capacitor C_{dc}.

Making use of (2), the inductor current peak value can be obtain as a function of V_p, V_{dc} and I_{b0} as:

$$I_{Lp} = \frac{2V_{dc} I_{bo}}{V_p} \tag{3.6}$$

The components of the boost converter are:

C_{dc}= 400microF, and L_b=2mH.

The input ac-voltage= 240V which gives rise to peak-dc value of 339.4V

V_{dc}=V_{bo}=400V.

3.2.2 The design of LLC resonant converter

For the resonant converter stage, the design procedure of the LLC Resonant Converter model used is presented here. As mentioned earlier, its suitability for high voltage and high-frequency applications and its advantage of allowing the regulation of output voltage at different load conditions are considered for its selection. This sub-section therefore describes the parameter selection procedures used for the designed LLC resonant half-bridge converter.

The LLC resonant converter's nonlinear circuit is changed to its ac-equivalent circuit as shown in Fig. 3.3. This is based on first harmonic approximation (FHA) approach. It makes the analysis of the initial complex circuit easy.

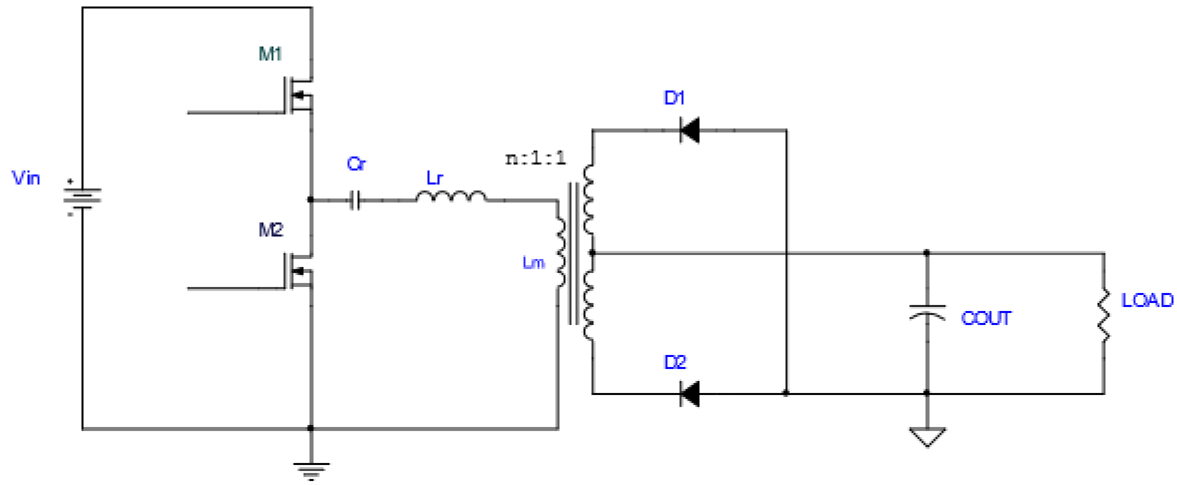

Fig.3.2: DC-DC Half-Bridge LLC Resonant Converter Circuit

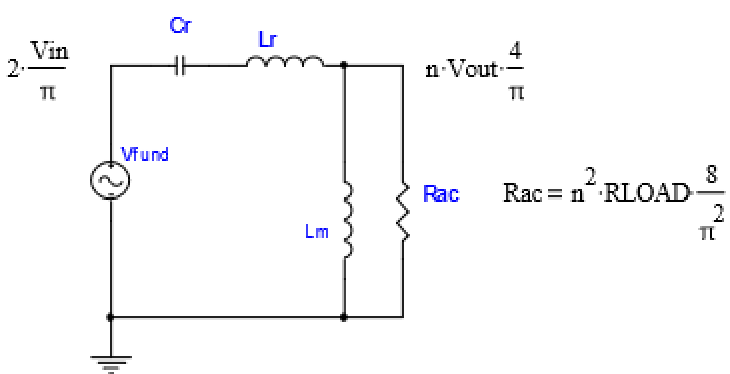

Fig.3.3: LLC Resonant Converter AC Equivalent Circuit

The resonant tank voltage input is a square wave and its amplitude equals to input DC voltage Vin. The square waveform fundamental component is:

$$\frac{2.V_{in}}{\pi}\sin(\varpi.t) \tag{3.7}$$

Also, the output square waveform fundamental component is given by:

$$\frac{4.n.V_{out}}{\pi}\sin(\varpi.t) \tag{3.8}$$

Power dissipation on the equivalent AC resistor is given by:

$$\frac{V_{out}^2}{R_{LOAD}} = \frac{\left(\dfrac{4.n.V_{out}}{\sqrt{2}\pi}\right)^2}{R_{ac}} \tag{3.9}$$

Making the AC resistor the subject of formula gives:

$$R_{ac} = \frac{8.n^2}{\pi^2}R_{LOAD} \tag{3.10}$$

The equivalent circuit transfer ratio is written as:

$$M = \left| \frac{\dfrac{j.w.L_m.R_{ac}}{j.w.L_m + R_{ac}}}{j.w.L_r + \dfrac{1}{j.w.C_r} + \dfrac{j.w.L_m.R_{ac}}{j.w.L_m + R_{ac}}} \right| \tag{3.11}$$

Therefore:

$$M = \left| \frac{1}{1 + \dfrac{L_r}{L_m} - \dfrac{1}{w^2.L_m.C_r} + \dfrac{j.w.L_r}{R_{ac}} - \dfrac{j}{w.C_r.R_{ac}}} \right| \tag{3.12}$$

As discussed earlier on, LLC converter has two resonant frequencies given as:

$$f_o = f_{r1} = \frac{1}{2\pi\sqrt{L_r C_r}} \tag{3.13}$$

$$f_1 = f_{r2} = \frac{1}{2\pi\sqrt{(L_r + L_m)C_r}} \tag{3.14}$$

The first one is determined by Lr and Cr, while the second is determined by Lp and Cr.

Since ZVS is anticipated for the LLC resonant converter, Eq. 7 shows the gain is unity at resonant

Also;

$$x = \frac{F_{sw}}{F_{r1}} \tag{3.15}$$

And;

$$\varpi = 2\pi F_{sw} = 2\pi . x . F_{r1} = \frac{x}{\sqrt{L_r . C_r}} \tag{3.16}$$

And the inductance ratio is defined as:

$$K = \frac{L_m}{L_r} \tag{3.17}$$

The ac equivalent load resistance is as defined in equation (3.10), that is;

$$R_{ac} = \frac{8 . n^2 . R_{LOAD}}{\pi^2}$$

And the quality factor is defined as:

$$Q = \frac{2\pi F_{r1} . L_r}{R_{ac}} = \frac{1}{2\pi F_{r1} . C_r . R_{ac}} \tag{3.18}$$

Therefore, voltage gain, M can be simplified as:

$$M = \left| \frac{1}{1 + \frac{1}{K} . \left(1 - \frac{1}{x^2}\right) + j.Q.\left(x - \frac{1}{x}\right)} \right| \tag{3.19}$$

Or;

$$M = \frac{1}{\sqrt{\left[1+\frac{1}{K}.\left(1-\frac{1}{x^2}\right)\right]^2+\left[Q.\left(x-\frac{1}{x}\right)\right]^2}} \tag{3.20}$$

From the equivalent cct of Fig. 3.3, Voltage gain (M) is also equal to the voltage output to voltage input ratio:

$$M = \frac{n.V_{out}.\frac{4}{\pi}}{2.\frac{V_{in}}{\pi}} = \frac{V_{out}}{V_{in}}.2.n \tag{3.21}$$

Therefore, the conversion ratio of voltage output to voltage input is written as:

$$\frac{V_{out}}{V_{in}} = \frac{M}{2.n} \tag{3.22}$$

For the second stage design, the schematic diagram of Fig. 3.2 is used as a reference. The input is supplied from PFC pre-regulation which comes directly from the output of the ac-dc stage. An LLC resonant converter with 2200W/250V output is proposed for this design work. The specifications used are listed thus:

- Nominal voltage input: 400VDC

- Output voltage: 250V/8.8A (2.2KW)

- Hold-up time requirement: 0.4ms (60Hz.)

- DC link capacitor, C_{dc}: 50µF

An estimation of the power efficiency is needed to obtain the maximum power input with the required design output power of 2.2KW.

Therefore, the maximum power input is obtain by:

$$p_{in} = \frac{p_o}{E_{ff}} \tag{3.23}$$

$$\therefore P_{in} = \frac{2200}{0.92} = 2391W$$

The maximum voltage input is given by:

$$V_{in}^{\max} = V_{O.PFC} \tag{3.24}$$

$$\therefore V_{in}^{\max} = 400V$$

Where $V_{o.pfc}$ is the nominal PFC voltage output. The minimum voltage input can be obtained by:

$$V_{in}^{\min} = \sqrt{V_{O.PFC}^{2} - \frac{2P_{in}T_{HU}}{C_{DL}}} \tag{3.25}$$

$$\therefore V_{in}^{\min} = \sqrt{400^2 - \frac{2x2391x0.4x10^{-3}}{50x10^{-6}}} = 349V$$

Where T_{HU} represents the hold-up time and C_{DL} represents dc-link capacitor

From Eq. (15), the recommend range of inductance ratio, K between Lm and Lr is from 3 to 10. It is chosen as 5 in this design.

In order to obtain the minimum and maximum voltage gain for the resonant network;

$$M^{\min} = \frac{V_{RO}}{V_{in}^{\max}/2} = \sqrt{\frac{K}{K-1}} = \sqrt{\frac{5}{5-1}} = 1.12$$

Where V_{RO} = reflected output voltage

$$M^{\max} = \frac{V_{in}^{\max}}{V_{in}^{\min}} M^{\min} = \frac{400}{349} .1.12 = 1.28$$

The transformer turns ratio can be obtain as:

$$n = \frac{N_p}{N_s} = \frac{V_{in}^{\max}}{2(V_o + V_F)} .M_{\min} \tag{3.26}$$

V_F = secondary side rectifier diode voltage drop.

Choosing $V_F = 0.9V$;

$$n = \frac{N_p}{N_s} = \frac{V_{in}^{\max}}{2(V_o + V_F)} .M_{\min} = \frac{400}{2(250+0.9)} .1.12 = 0.8928$$

In order to obtain the equivalent load resistance, equation (3.10) can be written as;

$$R_{ac} = \frac{8n^2}{\pi^2} \frac{V_o^2}{P_o} \tag{3.27}$$

Therefore;

$$R_{ac} = \frac{8n^2}{\pi^2} \frac{V_o^2}{P_o} = \frac{8x0.9^2 x250^2}{\pi^2 x2200} = 18.4\Omega$$

As calculated above, the maximum gain, M^{max} = 1.28 and making use of 15% margin, the needed peak gain will be M^{max} + 15% x M^{max} = 1.28 + 0.192 = 1.47

Making use of the peak gain curve, with k chosen as 5 and peak gain=1.47, then Q=0.4. This is shown in figure 3.4 below.

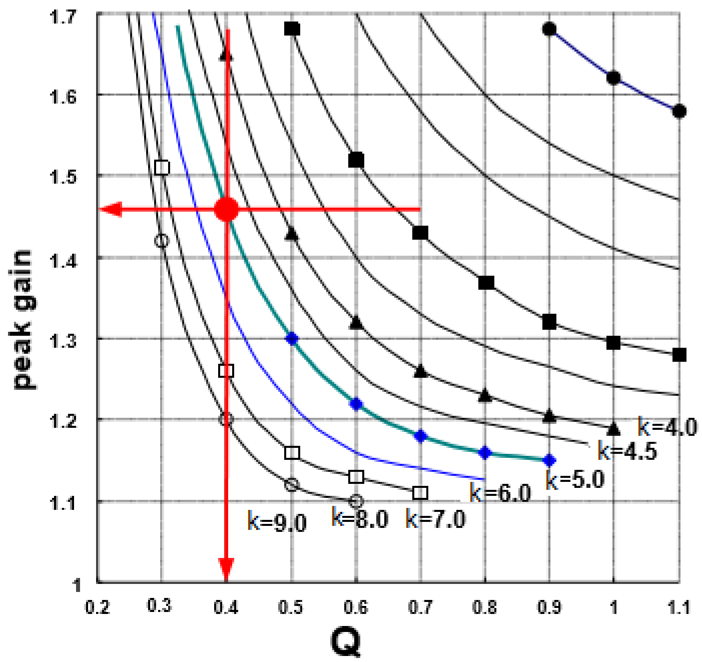

Fig.3.4: Design of Resonant Network with Peak Gain Curve for k=5

In order to obtain the resonant parameters;

$$C_r = \frac{1}{2\pi Q.\, f_o.\, R_{ac}} \tag{3.28}$$

$$L_r = \frac{1}{(2\pi f_o)^2 C_r} \tag{3.29}$$

$$L_m = K.\, L_r \tag{3.30}$$

Therefore, making use of equations (3.28), (3.29) and (3.30) we have:

$$C_r = \frac{1}{2\pi Q.\, f_o.\, R_{ac}} = \frac{1}{2\pi .0.4.150x10^3 .18.4} = 144nF$$

$$L_r = \frac{1}{(2\pi f_o)^2 C_r} = \frac{1}{\left(2\pi .150x10^3\right)^2 .144x10^{-9}} = 7.8\mu H$$

$$L_m = K.L_r = 39\mu H$$

Thus, for this design, making use of the steps above with resonant frequency f_{r1}= 150kHz, turns ratio n = 0.8928, C_o= 50x10^{-6}F. Using Q= 0.4 for K=5, the tank parameters calculated above are summarily given as;

$$C_r = 144nF, L_r = 7.8\mu H, and\ L_m = 39\mu H$$

3.3 Other Investigated Models

This section highlights the other LLC resonant converter topologies investigated in this research work for the purpose of comparatively analyzing them with the first and main model designed above. All are investigated for 2.2KW output power.

3.3.1 Boost and LLC-L model

The first and main one being an improved version of LLC series resonant converter. That is LLC-L resonant converter.

For LLC-L improved topology, a secondary side inductor (Ls) is connected in series with the resonant tank of LLC circuit on the transformer's secondary side before the secondary rectification section (Tan & Ruan, 2016). The resonant tank for an LLC-L resonant converter is depicted in fig. 3.5 below.

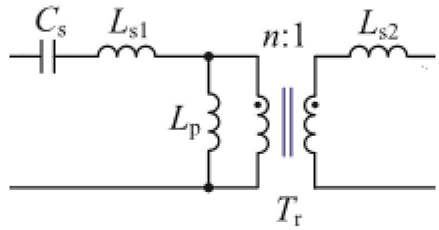

Fig.3.5: LLC-L Resonant Tank

For the design of this resonant circuit and the calculations of its component, the equivalence relations of two-port networks had to be made used of in order to obtain the equivalence relations of the resonant tanks of the first model and the subsequent models in this work.

Considering the two-port networks R1 and R2 of figure 3.6 below:

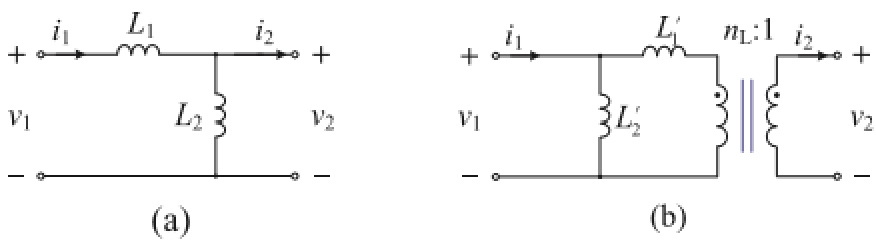

Fig.3.6: Two-Port Networks with Two Inductors. (a)R1.(b)R2

v_1, v_2, i_1 and i_2 represent the terminal voltages and currents of R1 and R2. These contains abundant harmonics and the phasor for the kth harmonics of v_1, v_2, i_1 and i_2 are represented by $\dot{V}_{1k}, \dot{V}_{2k}, \dot{I}_{1k}, and\ \dot{I}_{2k}$, respectively. Using figure 3.6(a), from the kth harmonic domain;

$$\begin{cases} \dot{V}_{1k} = \dot{V}_{2k} + jkwL_1\dot{I}_{1k} \\ \dot{I}_{1k} = \dot{V}_{2k} / (jkwL_2) + \dot{I}_{2k} \end{cases} \tag{3.31}$$

This can be written as:

$$\begin{bmatrix} \dot{V}_{1k} \\ \dot{I}_{1k} \end{bmatrix} = \begin{bmatrix} (L_1 + L_2)/L_2 & jkwL_1 \\ 1/(jkwL_2) & 1 \end{bmatrix} \begin{bmatrix} \dot{V}_{2k} \\ \dot{I}_{2k} \end{bmatrix} \tag{3.32}$$

Also, (3.32) can be written as:

$$\begin{bmatrix}\dot{V}_{1k}\\ \dot{I}_{1k}\end{bmatrix}=\begin{bmatrix}1 & jkw\frac{L_1(L_1+L_2)}{L_2}\\ \frac{1}{jkw(L_1+L_2)} & \frac{L_1+L_2}{L_2}\end{bmatrix}x\begin{bmatrix}\frac{L_1+L_2}{L_2} & 0\\ 0 & \frac{L_2}{L_1+L_2}\end{bmatrix}\begin{bmatrix}\dot{V}_{2k}\\ \dot{I}_{2k}\end{bmatrix} \quad (3.33)$$

Making:

$$\begin{cases}L_1^{/}=L_1(L_1+L_2)/L_2\\ L_2^{/}=L_1+L_2\\ n_L=(L_1+L_2)/L_2\end{cases} \quad (3.34)$$

Substituting (3.34) into (3.33) yields:

$$\begin{bmatrix}\dot{V}_{1k}\\ \dot{I}_{1k}\end{bmatrix}=\begin{bmatrix}1 & jkwL_1^{/}\\ \frac{1}{jkwL_2^{/}} & \frac{L_1^{/}+L_2^{/}}{L_2^{/}}\end{bmatrix}x\begin{bmatrix}n_L & 0\\ 0 & \frac{1}{n_L}\end{bmatrix}\begin{bmatrix}\dot{V}_{2k}\\ \dot{I}_{2k}\end{bmatrix} \quad (3.35)$$

And (3.35) can be written as:

$$\begin{cases}\dot{V}_{1k}=n_L\dot{V}_{2k}+jkwL_1^{/}\frac{\dot{I}_{2k}}{n_L}\\ \dot{I}_{1k}=\frac{\dot{V}_{1k}}{jkwL_2^{/}}+\frac{\dot{I}_{2k}}{n_L}\end{cases} \quad (3.36)$$

Making use of Eq. (3.34) and other resonant tank equivalence relations as given in (Tan and Ruan, 2016), it can be derived that:

$$\begin{cases}L_{s1}=L_s^{/}+L_p^{/}-\sqrt{(L_s^{/}+L_p^{/})L_p^{/}}\\ L_{s2}=\frac{L_p^{/}}{n^{/2}}\left(1-\sqrt{L_p^{/}/(L_s^{/}+L_p^{/})}\right)\\ L_{s3}=\sqrt{(L_s^{/}+L_p^{/})L_p^{/}}\\ n=n^{/}\sqrt{(L_s^{/}+L_p^{/})/L_p^{/}}\end{cases} \quad (3.37)$$

Making reference to the values of the parameters obtained in model1;

Where $L_r=L_s^{/}$, $L_m=L_p^{/}$ and $n^{'}=0.8928$

And substituting the values in Eq. (37) gives:

L_{s1}=4.1 μH

L_{s2}=4.3 μH

L_p=42.7 μH

N =0.978

The resonant capacitance value is maintained as 144nF
These are used in the design of the resonant circuit for the LLC-L model.

3.3.2 Boost and CLL model

Other models designed and simulated in the case of this research are analysed based on change in the resonant tank configurations with the different tanks shown in Fig. 3.6 below.

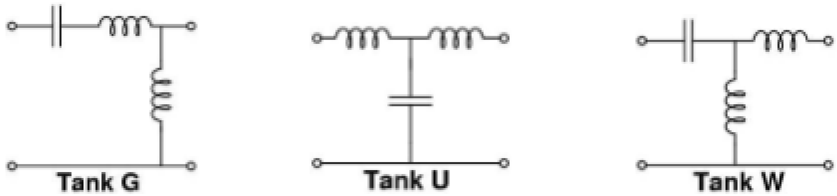

Fig.3.7 Resonant Tanks G, U and W.

Tank G is exactly the same as in LLC resonant converter of model1. Therefore using the same resonant component values gives the same output waveforms. In the case of Tank W, the design is taken to be similar to that of CLL resonant tank as depicted in Fig. 3.8 below

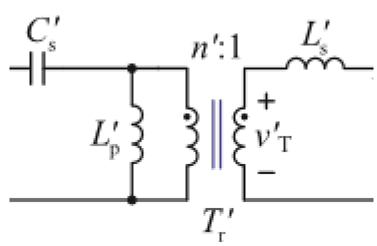

Fig.3.8: CLL Resonant Tank

This is done in order to make easy the derivations for the resonant components. For CLL resonant converter tank of figure 3.8 above, $L_s^{/}$ can be reflected to the primary side as as $n^{/2}L_s^{/}$,so that the resonant tank becomes the same as tank W as in figure (3.7).

In order to obtain the values of the resonant tank components for tank W, equation (3.38) is derived from equation (3.4) as shown in [32].

$$\begin{cases} L_s^{/} = L_s L_p \big/ \left[n^2\left(L_s + L_p\right)\right] \\ L_p^{/} = L_s + L_p \\ n^{/} = n\left(L_s + L_p\right)/ L_p \end{cases} \tag{3.38}$$

Using the values gotten in model 1 as done for the LLC-L model;

Where $L_r = L_s$, $L_m = L_p$ and $n^{'} = 0.8928$

$L_s^{/}= 8.2\text{x } 10^{-6}H$

$L_p^{/}= 46.8\text{x}10^{-6}H$

$n^{/} = 1.07$

The resonant capacitance value is maintained as $144\text{x}10^{-9}F$

These are used in the design of the resonant circuit for the W tank model.

3.4 Loss Determination

This section is committed to losses determination in the converter and also the choice of suitable transformer for the specific application being described in this thesis work. The transformer design procedure will be examined and also the losses calculation will be carried out.

3.4.1 Transformer design

The transformer design is pretty enormous and complex yet is highly needed, since the design and choosing of magnetics is capable of affecting the picking and expenses of every other power components in the converter, asides the influence exerted on overall performance and bigness or volume of the converter itself (Maniktala, 2012). There is the need for a careful design must be carried out carefully in order to minimize transformer losses. Transformer's loss is primarily categorized into two namely copper loss and core loss. These can be quantified and investigated through careful design from the appropriate calculations and better components selection.

This design procedure starts with determination of number of turns, due to the presence of two or more windings, which depends on the application, which are to be designed

The magnetic flux density of the material used must be taken into consideration during the design of the primary side number of turns. This is necessary to avert the core saturation, because number of turns at the primary side determines the peak of core's flux density denoted by 'Bcore'.

By making use of Michael Faraday's law, number of turns or flux at the primary side can be obtained. Given that:

$$e(t) = N\frac{d\phi}{dt} \tag{3.39}$$

Where $\frac{d\phi}{dt}$ represents the time derivative of the core's magnetic flux

$$\Rightarrow V(t) = N\frac{dB}{dt}A_m \tag{3.40}$$

Where A_m represents the core's effective area

$$B = \hat{B}\cos wt \Rightarrow V_1(t) = N_1 A_m \frac{d\hat{B}}{dt}\cos(wt) \tag{3.41}$$

$$\Rightarrow V_1(t) = N_1 A_m wB\sin(wt) \tag{3.42}$$

$$\Rightarrow V_1 = N_1 A_m w B_{core} \tag{3.43}$$

$V_1(t)$ is the primary side time-varying voltage

Magnetic flux is therefore obtained as:

$$\Phi = A_m \hat{B}_{core} \tag{3.44}$$

Putting equation (3.44) into (3.40) yields:

$$\int_0^{DTs} V_1 dt = N_1 A_m \int_{-B_{core}}^{B_{core}} dB \tag{3.45}$$

The primary side applied voltage during the interval of active power transfer is V_1, and it is equal to the voltage input. This is what produces the peak flux density $\hat{B}_{core}$ in the transformer core. This always changes from negative to positive depending on the converter's operation as bidirectional of unidirectional one.

This therefore generates the equation below:

$$\Rightarrow N_1 = \frac{V_d DT_s}{2A_m \hat{B}_{core}} \tag{3.46}$$

From equation (3.45), the input voltage applied over the transformer is a factor of the peak flux density. A change in duty cycle DT_s will also give rise to a change in $\hat{B}_{core}$ or N_1, depending on the calculation method.

Obtaining a suitable transformer core requires the consideration of both the maximum duty cycle $(D_{\max})$ and the maximum input voltage $(V_{d,\max})$.

$$\Rightarrow N_1 = \frac{V_{d,\max} D_{\max} T_s}{2 A_m \hat{B}_{core}} \tag{3.47}$$

Change in duty cycle results into change in the maximum flux density and also smaller core loss. A suitable transformer's size can be chosen using any of these two methods:

[1] Specify the number of turns and obtain the flux levels from calculations and confirm their occurrence in the core;

[2] Specify the flux levels and obtain the number of turns through calculations and confirm their fitting to the core.

A vital point to be observed from Eq. (3.47) is that the peak flux density reduces when the number of turns on the primary side is increased. This in turn reduces the core losses, although there is increase in the copper losses. Obviously, there is usually a concession between the core and copper losses. Although from the ideal sense, losses in transformers should proportionally be divided into core and copper losses equally, in reality, achieving this is hard. Therefore, the balance that exists between them should be kept while the difference which gives the smallest deviation will assure the most efficient transformer operation

For the calculation of the wiring cross-sectional, the RMS currents on the transformer's both sides must be known. These are gotten by making use of the fundamental equation spelt out in (Mohan, Underland, & Robbins, 2003). Since the operating frequencies used in this project are quite high, in order to reduce the skin and proximity effects losses in conductors Litz wire is utilized. It comprises of several thin wire strands, insulated separately and twisted together.

In practical construction of transformers used in applications with high operating frequencies as in this thesis work, litz wire is suggested. This helps in reducing conductors' proximity and skin effects losses. Litz wire comprises of several thin wire strands which are insulated separately and twisted together (Mohan et al., 2003).

Since the transformer consists of relatively high currents, a litz wire of 0.94mm^2 can be utilized for this application. Also a current density of 3A/mm^2 or 4A/mm^2 can be chosen.

In transformer design, one of the most problematic part is the minimum switching frequency condition and it takes place at full load and minimum input voltage. In order to obtain this minimum switching frequency, gain curve can be plotted making use of the gain Eq. (3.19). Through this, minimum switching frequency can be obtained. Thus, the minimum number of turns for transformer primary side is gotten by:

$$N_p^{\min} = \frac{n(V_o + V_F)}{2 f_s^{\min} \,.\, M_V \,.\, \Delta B \,.\, A_e} \tag{3.48}$$

Where A_e represents the cross-sectional area of the transformer core in meter square, and

ΔB represents the maximum flux density swing in Tesla. This is illustrated in Fig. 3.9 Below.

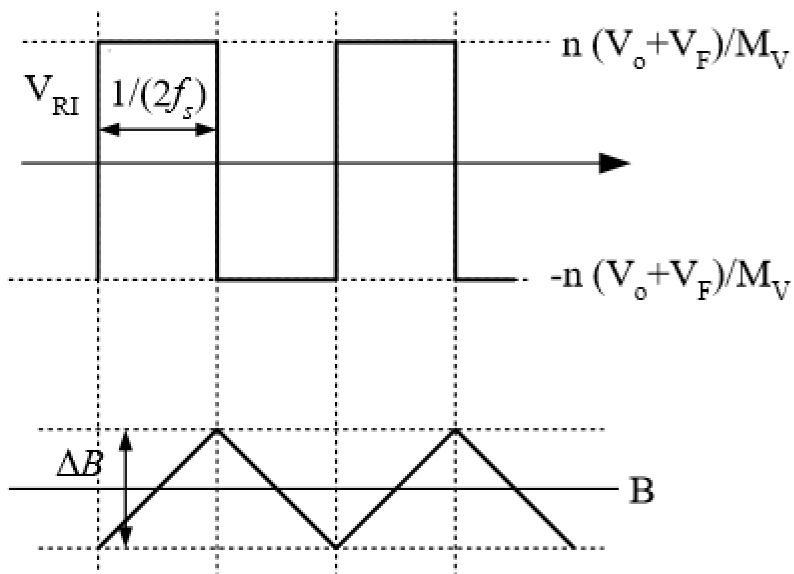

Fig.3.9: Flux Density Swing

For absence of reference data, range of ΔB from 0.3 to 0.4 can be used. M_V represents virtual gain which is as a result of leakage inductance at the secondary side.

For the design in this work, ΔB is taken as 0.4.

Therefore using Eq. (3.48):

$$N_p^{\min} = \frac{n(V_o + V_F)}{2 f_s^{\min} \,.\, M_V \,.\, \Delta B \,.\, A_e}$$

$$= \frac{1(250+0.9)}{2x78x10^3 x0.4x1.12x107x10^{-6}} = 34 turns$$

The number of wires for the transformer primary side is vital copper loss examination. The lizt wire are usually piled up in a bundle so as to stand the high current. The number of wires present in the bundle can therefore be calculated.

At the primary side, the number of wires is given as:

$$X_{pri}^{bundledwires} = \frac{I_{pri,rms}}{JA_{litz}} \tag{3.49}$$

Where J = wire current density.

The bundled conductor diameter can be obtained as:

$$A_{1,bundle} = X_{pri} A_{litz} \tag{3.50}$$

At the secondary side, the number of wires is given as:

$$X_{\sec}^{bundledwires} = \frac{I_{\sec,rms}}{JA_{litz}} \tag{3.51}$$

Also, the bundle conductor diameter can be obtained as:

$$A_{2,bundle} = X_{\sec} A_{litz} \tag{3.52}$$

The total winding area is now obtained. The copper filling factor, $K_{CU,}$ is taken to be equal to 0.5.

$$A_{winding} = \frac{A_{m1,bundle}N_1 + A_{2,bundle}N_2}{k_{cu}} \tag{3.53}$$

3.4.1.1 Core loss determination

Physical behavior of the magnetic material the transformer core is made of gives rise to the transformer's core loss. These core losses are generally referred to as eddy currents loss and hysteresis loss. It is expected that losses in the transformer core should exist, all the more at high frequencies. Ferrites are the commonly popular material for transformer core. According to (Mohan et al., 2003), core losses per unit volume is given by:

$$Corelossdensity = k\ x\ f_{sw}^{a}\ x\left(\Delta B_{\max}\right)^{b} \tag{3.54}$$

Core loss density needs to be scaled in terms of frequency and flux density.

The switching frequency f_{SW} is in kHz

B = peak flux density (in T)

k depends on material type. For ferrite materials, the losses are nearly proportional to f_{SW} (that is, a=1) and to flux density square (that is,b=2).

3.4.1.2 Copper loss determination

For calculation of transformer copper loss, the length of one L_{turn} turn which can be gotten from core datasheet must be obtained. After obtaining the windings number of turns, the total length of the conductors in both sides of the transformer can be calculated. Therefore;

$$L_{pri,wind} = L_{turn}N_1; L_{\sec,wind} = L_{turn}N_2 \tag{3.55}$$

The wires resistance on both transformer's sides can now be calculated as:

$$R_1 = \frac{\rho_{cu} L_{pri,wind}}{A_{1,bundle}} \tag{3.56}$$

$$R_2 = \frac{\rho_{cu} L_{\sec,wind}}{A_{2,bundle}} \tag{3.57}$$

The copper resistivity, $\rho_{cu}, = 1.7x10^{-8}\Omega m$

Total transformer's resistive losses is gotten as:

$$P_{cu} = R_1 I_{1,rms}^2 + R_2 I_{2,rms}^2 \tag{3.58}$$

While the transformer's maximum power dissipated is gotten as:

$$P_{tot} = P_{cu} + P_{core} \tag{3.59}$$

3.4.2 Semiconductors loss

Semiconductor losses can be split into two types. The first being switching losses that occur when the switch is been turned on and off. The second is conduction losses that take place during the conducting period of the switches. When conducting, the MOSFET is behaves like a resistor. It thus gives rise to some amount of conduction losses and these depend on the ON state resistance value of the MOSFET and also the current flowing through it.

$$P_{on-state} = R_{dson} I_{on}^2 \tag{3.60}$$

Practically though, generally there exists a body diode in the switch module, situated in anti-parallel to the MOSFET and it carries current with reverse polarity. This diode conducts and afterwards turns on the MOSFET and preparation for ZVS. Some ON state losses could also be generated due to forward voltage drop across the diode when it is on. These losses are also added with the MOSFET ON state losses to give rise to total conduction losses of the switch module. Therefore:

$$V_{on-state} = V_{sd} + R_{dson\, i_{on}} \tag{3.61}$$

$$P_{on-state} = \frac{1}{T_{sw}} \int_0^{T_{sw}} i_{on} \left(V_{sd} + R_{ds\, i_{on}} \right) dt =$$

$$= \frac{V_{sd}}{T_{sw}} \int_0^{T_{sw}} i_{on} dt + \frac{R_{dson}}{T_{sw}} \int_0^{T_{sw}} i_{on}^2 dt =$$

$$= V_{sd} I_{on(avg)} + R_{dson} I_{on(rms)}^2 \tag{3.62}$$

Both the ON state resistance of the switch module and forward voltage drop can be gotten from switch datasheet while the current’s average value and its rms can be individually calculated.

3.5 Resonant Capacitor Selection Approach

In selecting a suitable resonant capacitor, consideration of the current rating is important since a reasonable quantity of current passes through the capacitor. The RMS value of the current flowing through the capacitor can be obtain by:

$$I_{Cr}^{RMS} \cong \frac{1}{E_{ff}} \sqrt{\left[\frac{\pi I_o}{2\sqrt{2n}} \right]^2 + \left[\frac{n\left(V_o + V_F\right)}{4\sqrt{2} f_o M_v \left(L_p - L_r\right)} \right]^2} \tag{3.63}$$

Where during normal operation, the nominal voltage of resonant capacitor is obtain by:

$$V_{Cr}^{nom} \cong \frac{V_{in}^{\max}}{2} + \frac{\sqrt{2}\,.\,I_{Cr}^{RMS}}{2\,.\,\pi\,.\,f_o\,.\,C_r} \qquad (3.64)$$

But during overload condition or load transient, there is increase in the capacitor voltage. Therefore, in order to choose a suitable capacitor, the Over Current Protection (OCP) level is considered. The maximum resonant capacitor voltage is therefore gotten as:

$$V_{Cr}^{\max} \cong \frac{V_{in}^{\max}}{2} + \frac{I_{OCP}}{2\,.\,\pi\,.\,f_S^{\min}\,.\,C_r} \qquad (3.65)$$

For the calculations of model 1 in this paper;

$$I_{Cr}^{RMS} \cong \frac{1}{E_{ff}} \sqrt{\left[\frac{\pi I_o}{2\sqrt{2n}}\right]^2 + \left[\frac{n(V_o + V_F)}{4\sqrt{2}\, f_o M_v (L_p - L_r)}\right]^2} = 14.11 = 14A$$

At normal operation, the peak current at the primary side is:

$$I_{Cr}^{peak} = \sqrt{2}\,.\,I_{Cr}^{rms} = 19.8A$$

The over current protection level is set at 25% margin of the primary side peak current:

$$\Rightarrow I_{ocp} = \frac{25}{100} x 19.8 + 19.8 = 24.75 \approx 25A$$

Therefore;

$$V_{Cr}^{nom} \cong \frac{V_{in}^{\max}}{2} + \frac{\sqrt{2}\,.\,I_{Cr}^{RMS}}{2\,.\,\pi\,.\,f_o\,.\,C_r}$$

$$= \frac{400}{2} + \frac{\sqrt{2}\, x\, 14}{2\,.\,\pi\,.\,150x10^3\,.\,144x10^{-9}} = 345.88V$$

And;

$$V_{Cr}^{\max} \cong \frac{V_{in}^{\max}}{2} + \frac{I_{OCP}}{2\,.\,\pi\,.\,f_S^{\min}\,.\,C_r}$$

$$= \frac{400}{2} + \frac{25}{2\,.\,\pi\,.\,78x10^3\,.\,144x10^{-9}} = 554V$$

For the resonant capacitor design, 630V rated low-ESR film capacitor is appropriate.

3.6 Rectifier Network Design Approach

The utilization of the centre tap winding in the secondary side of the transformer gives rise to a diode voltage stress that is twice the value of the voltage output and is given as:

$$V_D = 2(V_o + V_F) \tag{3.66}$$

Also, the value of the RMS current through each of the rectifier diode is expressed as:

$$I_D^{RMS} = \frac{\pi}{4} I_o \tag{3.67}$$

By using equations (3.66) and (3.67), the voltage and current stress of the rectifier diode are obtained as:

$$V_D = 2(V_o + V_F) = 2(250 + 0.9) = 501.8V$$

$$I_D^{RMS} = \frac{\pi}{4} I_o = \frac{\pi}{4} x\, 8.8 = 6.9A$$

For this project, a 100V/20A Schottky diode will be appropriate for the rectifier stage, especially taking into consideration the voltage overshoot, an effect of stray inductance.

For the ouput capacitor, the ripple current flowing, its ripple voltage and the power loss can be investigated through the following expressions:

$$I_{Co}^{RMS} = \sqrt{\left(\frac{\pi I_o}{2\sqrt{2}}\right)^2 - I_o^2} = \sqrt{\frac{\pi^2 - 8}{8}} I_o \quad (3.68)$$

$$\Delta V_o = \frac{\pi}{2} I_o . R_c \quad (3.69)$$

$$P_{Loss.Co} = \left(I_{Co}^{RMS}\right)^2 . \; R_c \quad (3.70)$$

Where R_C represents the effective series (ESR) of the output capacitor.

From these three equations, the loss in the output capacitor of the models designed in this work can be estimated.

$$I_{Co}^{RMS} = \sqrt{\left(\frac{\pi I_o}{2\sqrt{2}}\right)^2 - I_o^2} = \sqrt{\frac{\pi^2 - 8}{8}} I_o = 4.254A$$

Therefore:

$$P_{Loss.Co} = \left(I_{Co}^{RMS}\right)^2 . \; R_c = (4.254)^2 \; . \; 0.04 = 0.72W$$

Where R_c is the effective series resistance (ESR) of the output capacitor.

3.7 Design Results

The different models designed for both stages of the EV battery charger are simulated using MATLAB/Simulink environment. The generated output waveforms which reveals their performance are analysed and discussed in the next chapter.

CHAPTER 4

RESULTS AND DISCUSSION

4.1 Parameters used in the MATLAB/Simulink

The designed EV charging systems all consists of two stages with the first stage being the same of all designed model, that is the rectifier and boost converter stage, while the the second stage consists of different resonant converter topologies for the different models designed.

Tables 4.1 and 4.2 show the simulation parameters used for the two stages of the EV battery charger designed for the research.

Table 4.1: Simulation Parameters for Ac-Dc Design Stage

s/n	Parameter	Value
1	Input grid voltage, Vac	240V
2	Output dc voltage	400v
3	Dc-link capacitance, C_{dc}	400μF
4	Boost inductor, L_b	2mH

Table 4.2: Simulation Parameters for Dc-Dc Resonant Converter Design Stage

s/n	Parameter	Value
1	Input voltage	400V
2	Output voltage	250v
3	Resonant capacitance	144*n*F
4	Resonant inductance	7.8 μH
5	Magnetizing inductance	39 μH
6	Output filter capacitance	50 μF
7	Resonant frequency	150kHz

4.2 Simulation Results and Output Waveforms verification

The designed simulated circuit of model 1 is shown in figure 4.1 below:

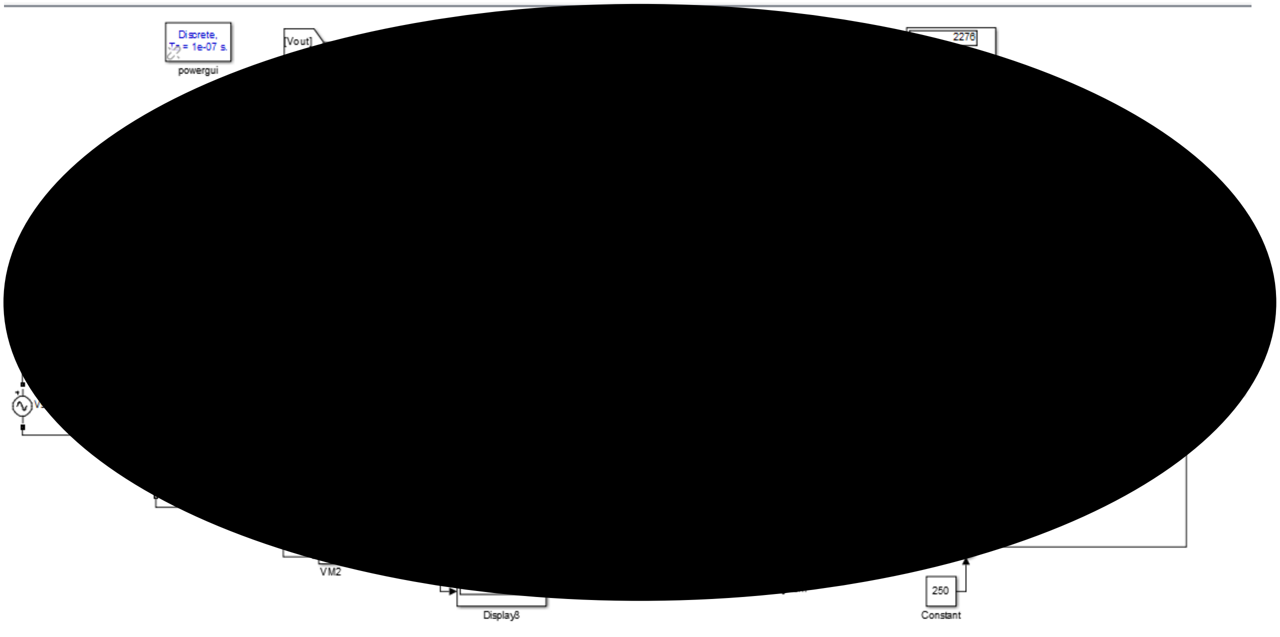

Fig. 4.1: Designed LLC Resonant Converter in MATLAB Simulink

The following waveforms are obtained from the simulated circuit for model 1:

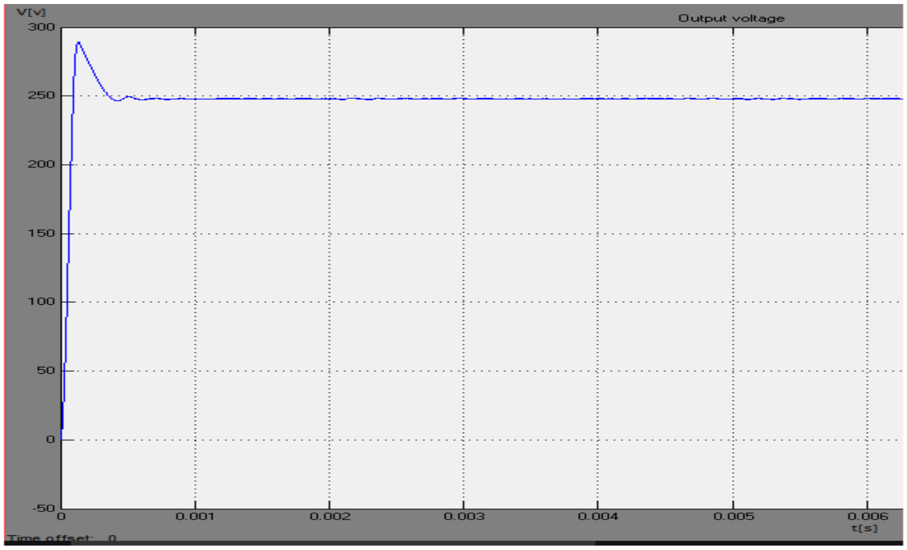

Fig 4.2: Output Voltage Waveform for Model 1

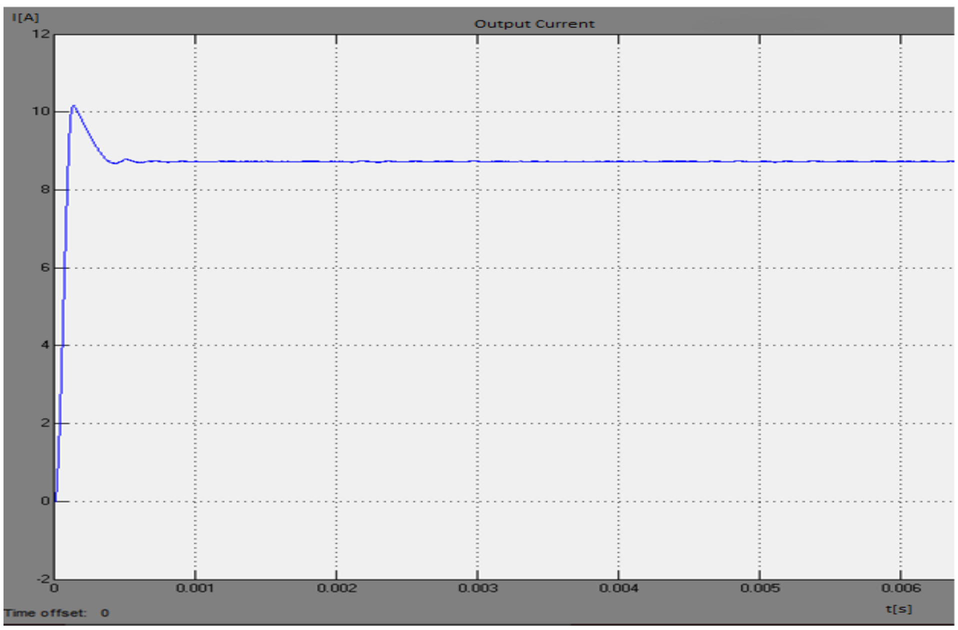

Fig 4.3: Output Current Waveform for Model 1

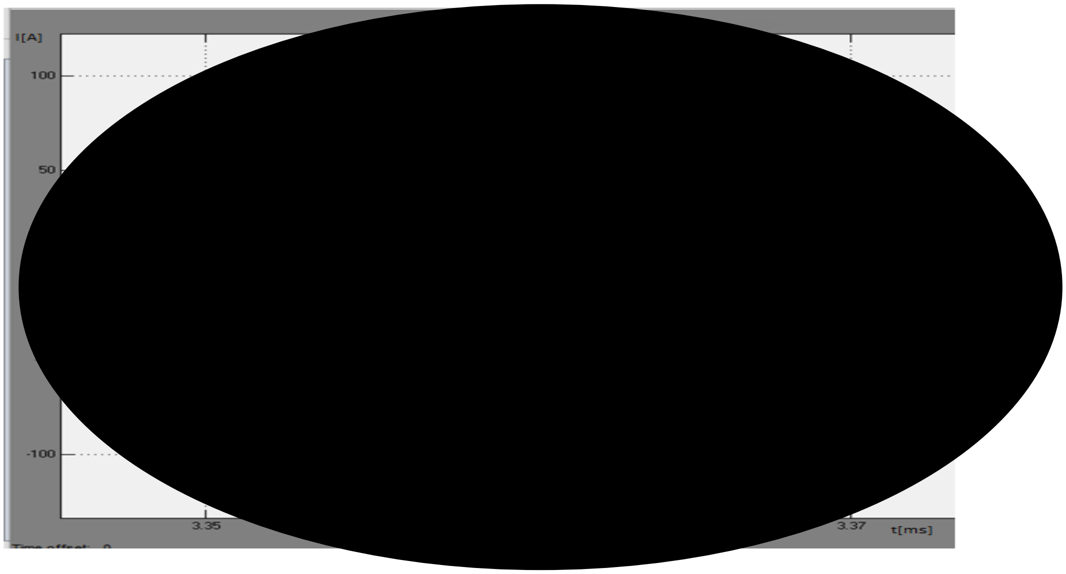

[redacted]

Fig 4.4: Resonant Current Waveform for Model 1

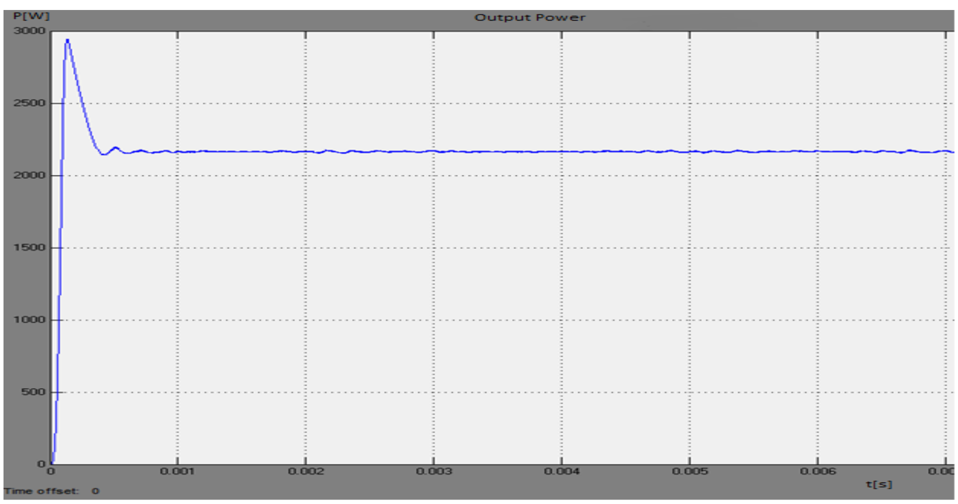

Fig 4.5: Output Power Waveform for Model 1

For the other models designed, the results are similar, especially with some modifications and improvement on the designed parameters. The CLL resonant waveforms are as shown below:

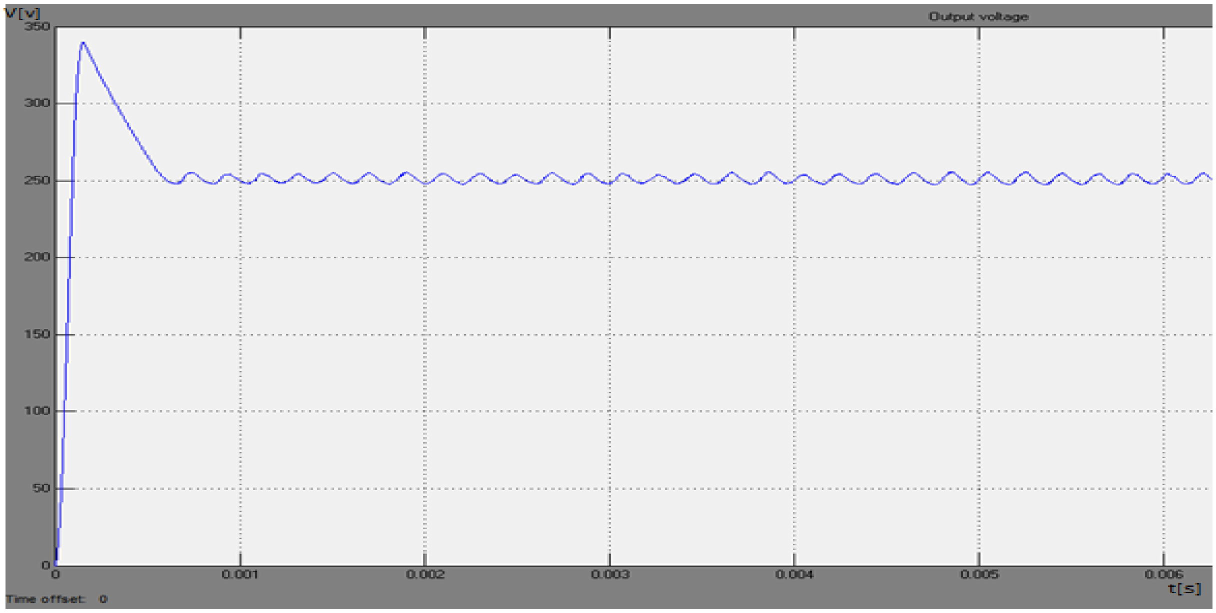

Fig 4.6: Output Voltage for Model 2 with CLL Resonant Tank

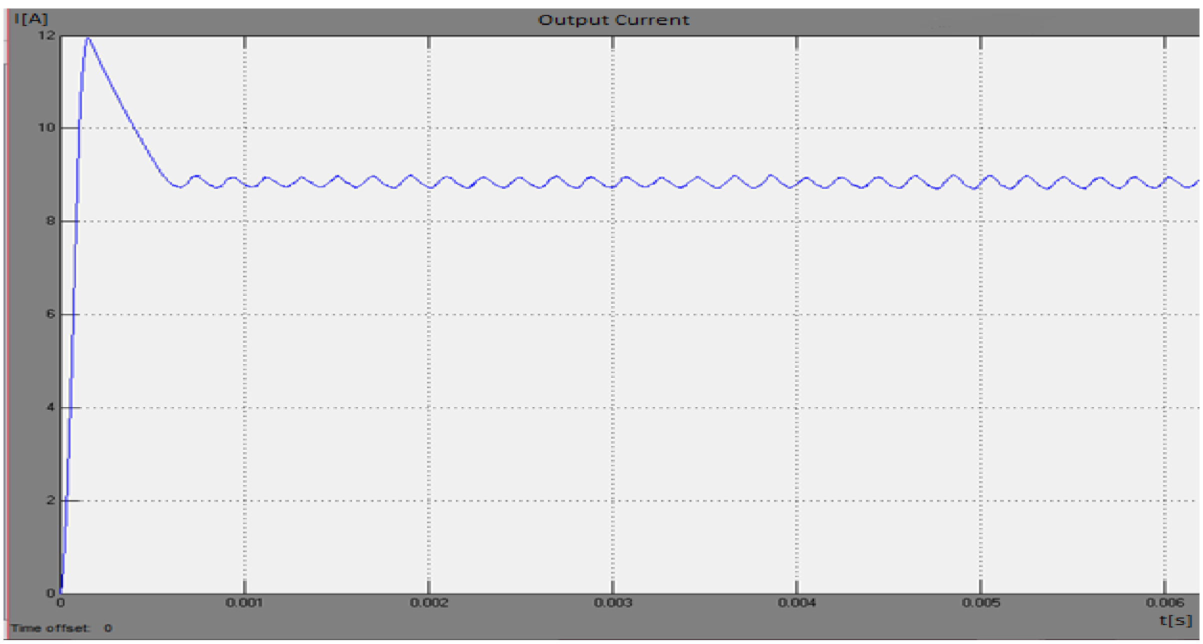

Fig 4.7: Output Current for Model 2 with CLL Resonant Tank

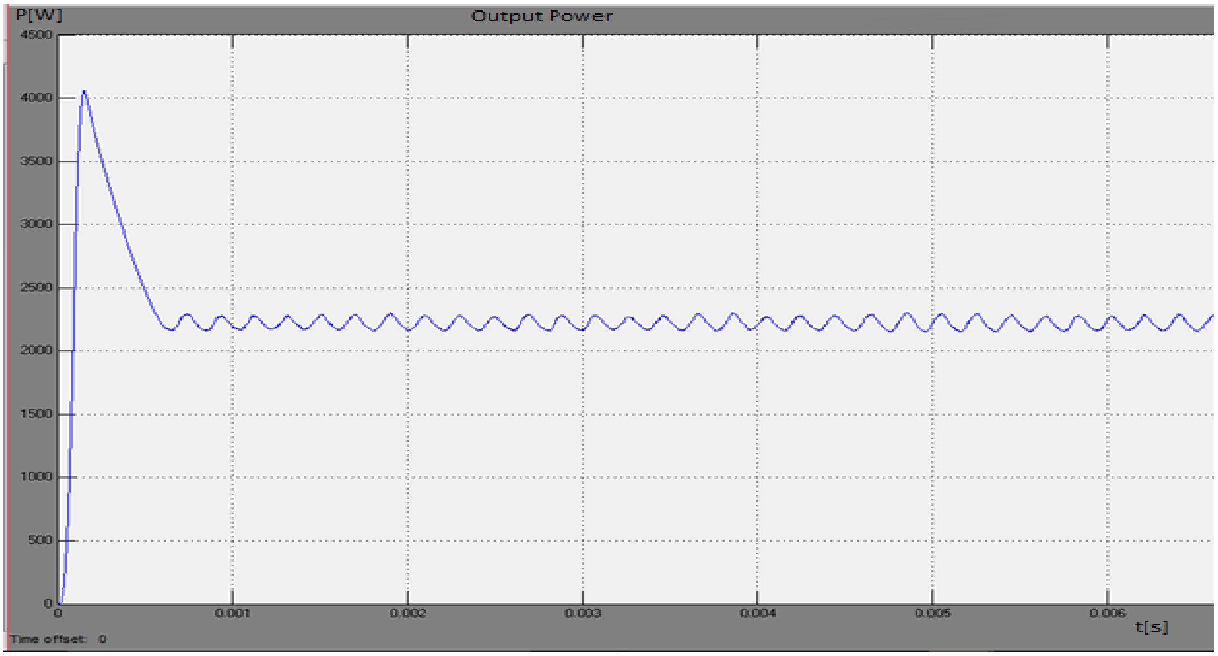

Fig 4.8: Output Power Waveform for Model 2 with CLL Resonant Tank

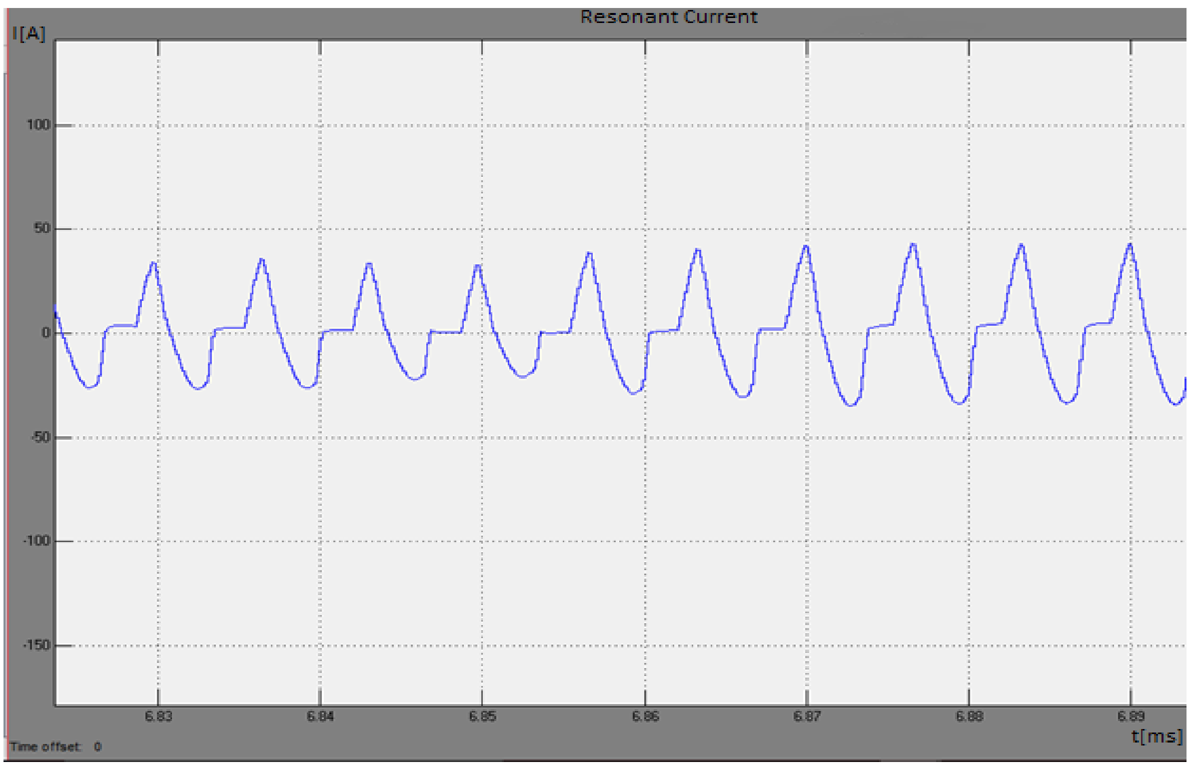

Fig 4.9: Resonant Current Waveform for Model 2 with CLL Resonant Tank

The LLC-L resonant waveforms are as shown below:

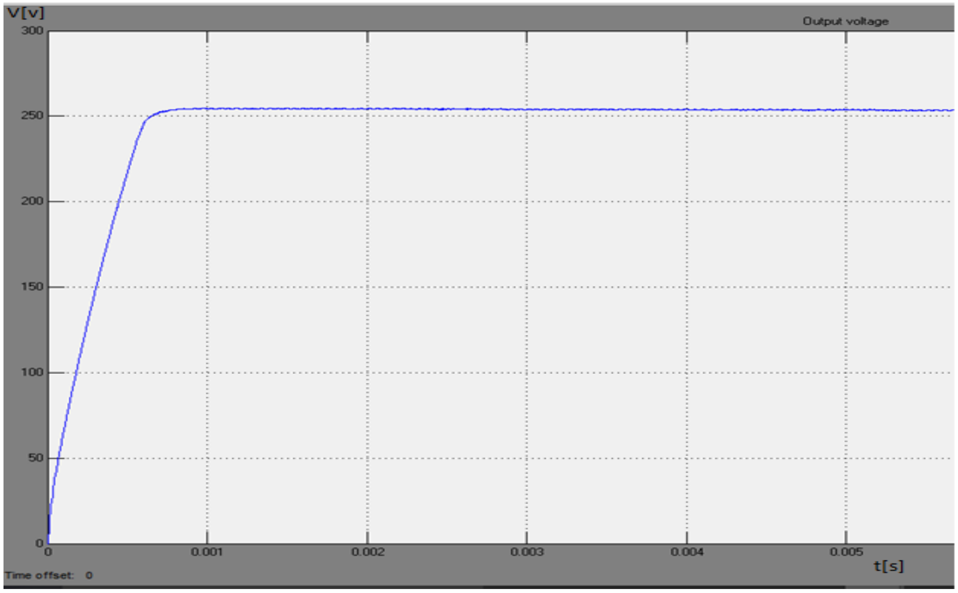

Fig 4.10: Output Voltage for Model 3 with LLC-L Resonant Tank

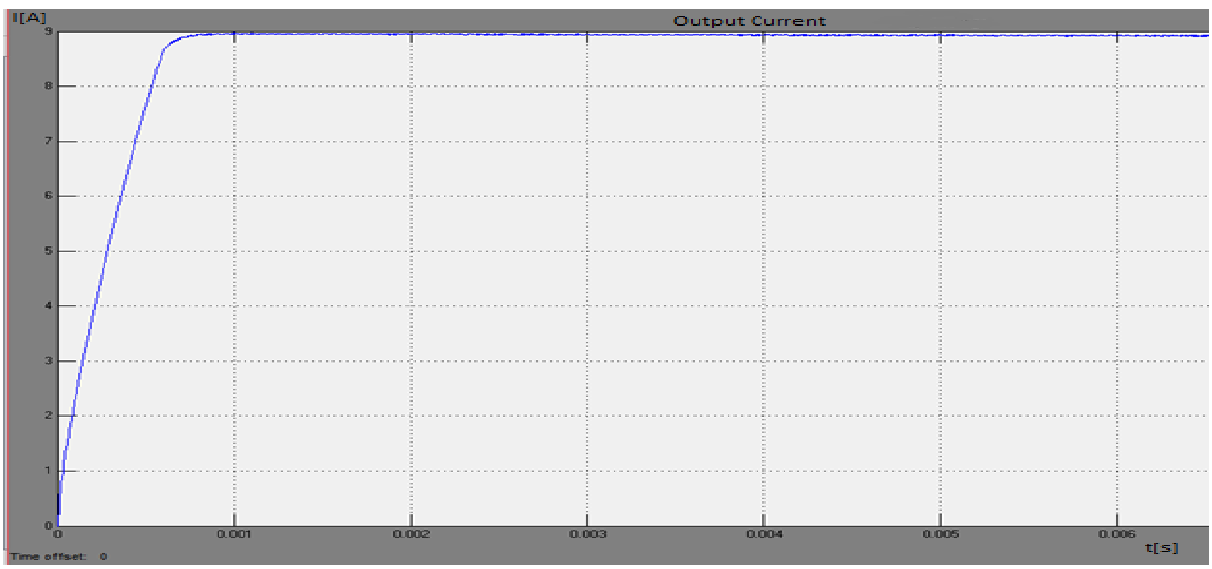

Fig 4.11: Output Current for Model 3 with LLC-L Resonant Tank

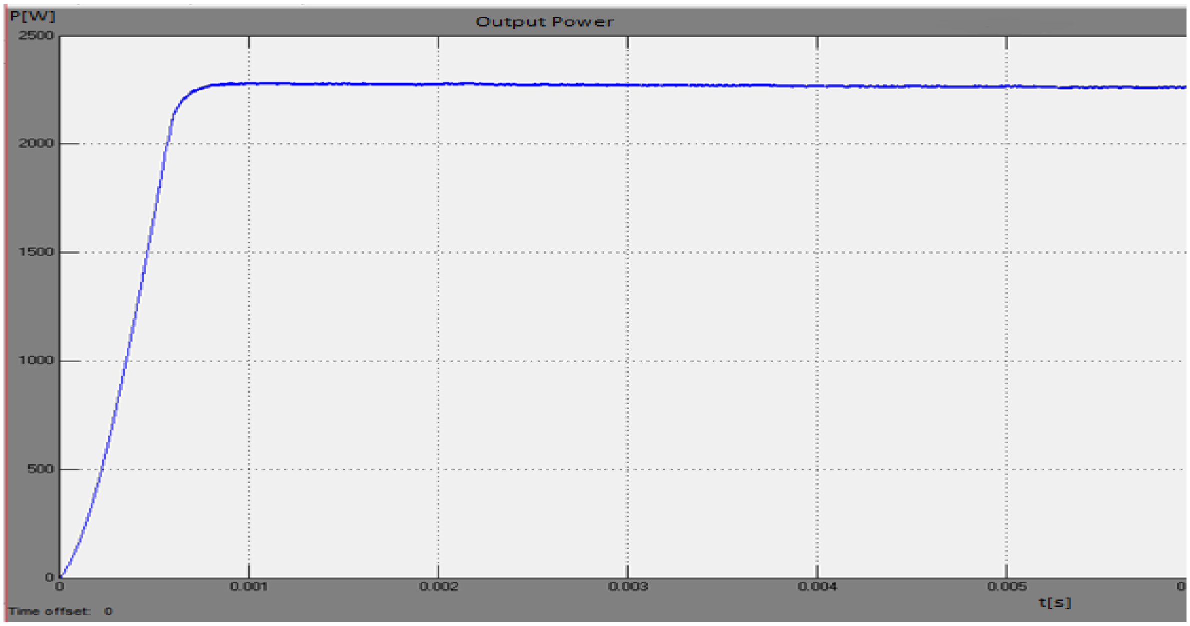

Fig 4.12: Output Power Waveform for Model 3 with LLC-L Resonant Tank

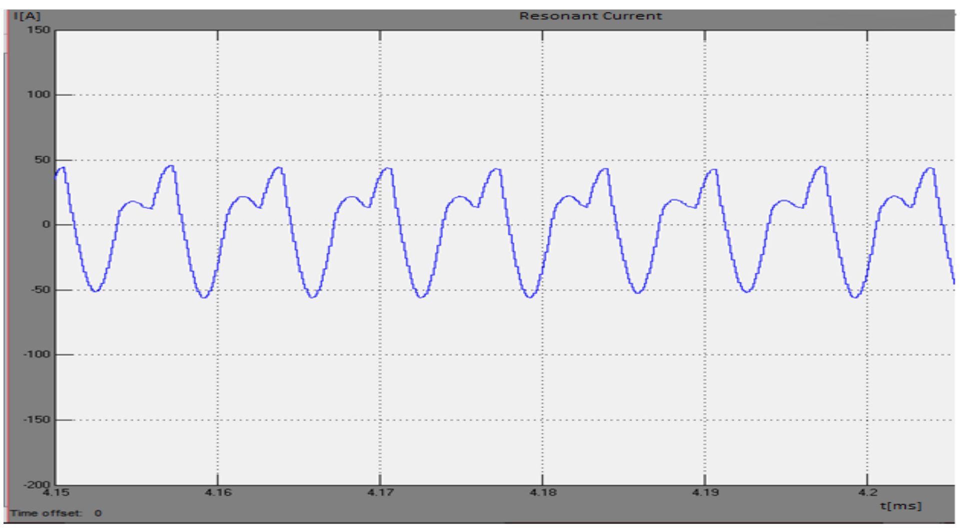

Fig 4.13: Resonant Current Waveform for Model 3 with LLC-L Resonant Tank

Fig. 4.14 below shows the simulation efficiency versus output current comparison at 240Vac input voltage of the three main models designed and simulated in this project. The efficiency of the boost_LLC model is very close to that of boost_CLL model. That of boost_LLC-L model is relatively distant and this is as a result of more core losses since it has a higher power density more than both the boost_LLC and boost_CLL models.

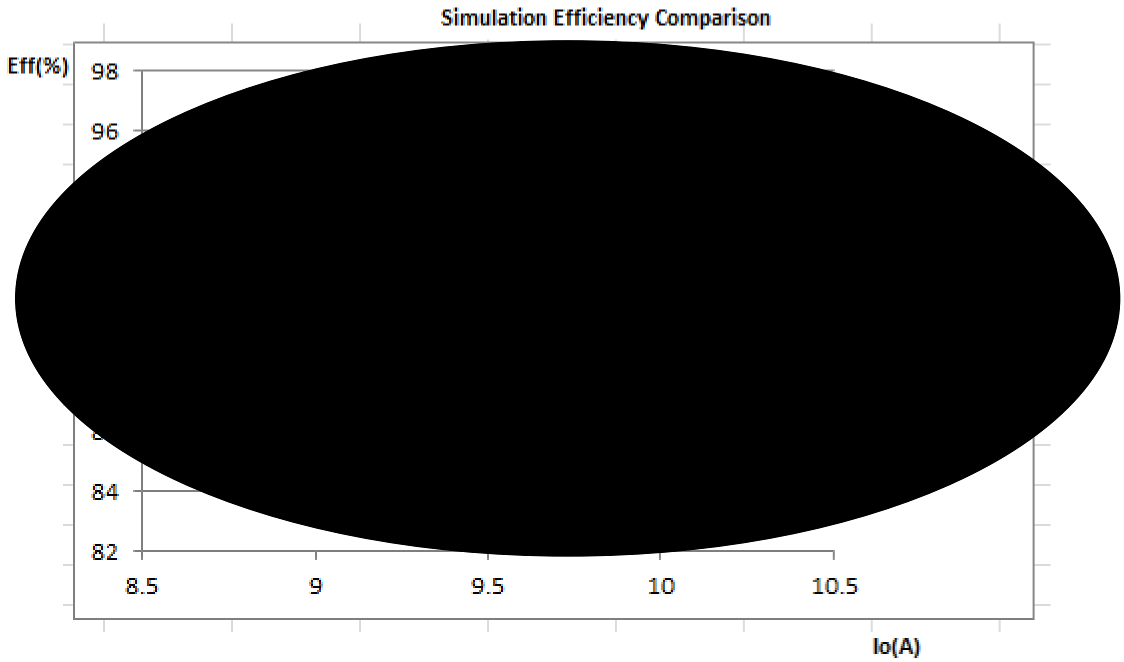

Fig 4.14: Efficiency of Boost_LLC, Boost_CLL and Boost_LLC-L Models at 240Vac input

Table 4.3: Efficiency, Volume and Loss comparison of the Designed Models

Model	Efficiency	Volume	Conduction Loss
Boost_LLC	Higher	Lower	Lower
Boost_CLL	High	Lower	High
Boost_LLC-L	Lower	Higher	Higher

Table 4.3 above shows the comparison between the three main EV charging models designed in this project. The boost_LLC combination has the highest efficiency and this is mainly as a result of less losses within the system. Also, the boost_LLC-L model is more voluminous than boost_LLC and boost_CLL models designed. This is partly due to the presence of the secondary

leakage inductor and also higher power density. This in turn increases the conduction loss within the system and therefore reduces the efficiency.

4.3 Boost_LLC Dynamic Response Consideration

Fig.4.15 below reveals how the charger controls the output-power (blue line colour) when there isvariation in the output voltage (denoted by red line colour). The output voltage is made to vary between the minimum value of 200V and maximum value of 260V since the battery voltage level utilized in EVs generally ranges between 200 and 390.

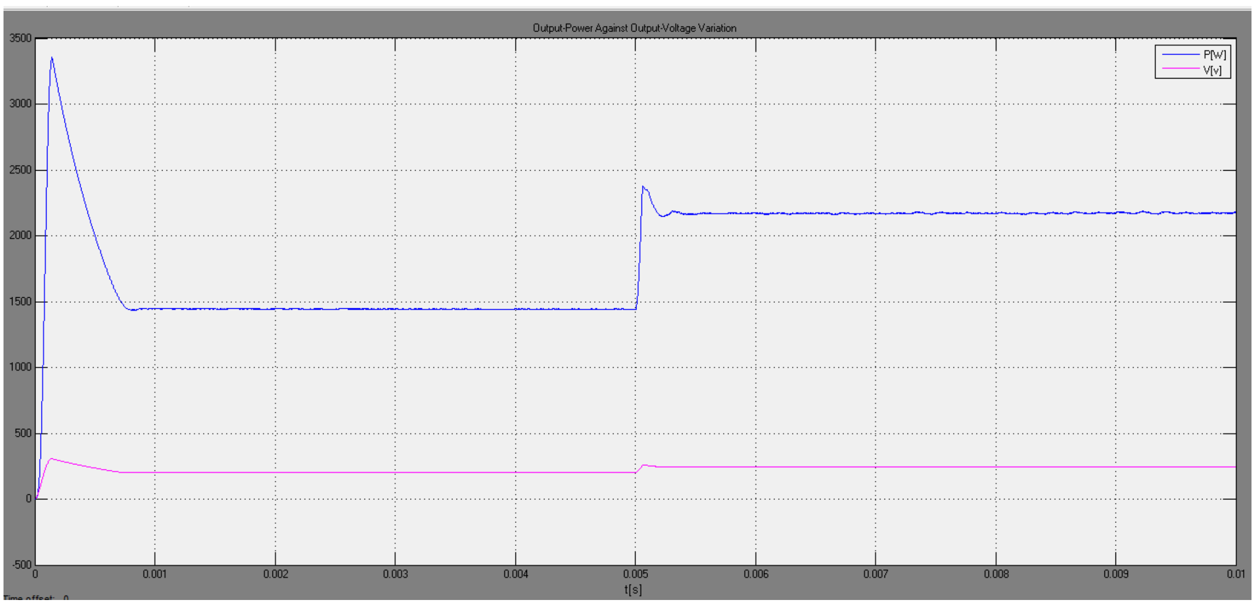

Fig 4.15 : Output-Power Response Against Output-Voltage Variation

4.4 Remarks and Discussion

From the simulations carried out on the different designed EV battery charger models, the charger configurations for both boost/LLC resonant converter, boost/CLL resonant converter and also boost/LLC-L resonant converter topologies and the other models with different/improved resonant tanks were designed and their performances were analyzed based on their output waveforms.

It is observed that the first model with [redacted] LLC resonant converter combination gives better output voltage wave[redacted] performance from the resonant current waveform. This [redacted] switching which therefore possesses some advanta[redacted] This re-emphasizes the inherent advantages [redacted] operation at very high frequencies [redacted]

It is also observe[redacted] and W, yielding better efficiency [redacted] is also better in aspects stated [redacted] requiring more improvement [redacted] current waveform of [redacted] as can be seen from the [redacted] and nearly perfect dead-tim[redacted]

Also, for the [redacted] with the bridge rectifier through [redacted] active power and the reactive [redacted] makes model1 a better option, unless [redacted] operation in order to annex the reactive [redacted] the resonant tank component values for both [redacted] resonant converters are higher, it makes both to have [redacted] converter.

CHAPTER 5

CONCLUSION AND FUTURE WORKS

This thesis focuses on the comparative [redacted] electric vehicle battery charger with output power of 2.2KW. The designe [redacted] onsists of two converter stages as it is an on-board EV [redacted] ifier and boost converter stage is the ac-dc st [redacted]

The second st [redacted] t topologies of resonant co [redacted] ies resonant converter) [redacted] verter and LLC res [redacted]

The E [redacted] th their perfo [redacted] ion at reso [redacted]

It ca [redacted] other reso [redacted] Zero volta [redacted]

It is a [redacted] C with tanks [redacted] also of good pe [redacted]

From this [redacted] t and LLC series resona [redacted] voltage, soft switching and [redacted] ency. It is also cost efficient due [redacted] with the boost and LLC-L resonant conv [redacted] charger of Model 1 is therefore a good candidate [redacted] with optimum performance and a high efficiency and the results [redacted] future promising candidate.

REFERENCES

Bhat, A. K. (1993). Analysis and Design of a Series-Parallel Resonant Converter. *IEEE Transactions on Power Electronics*, *8*(1), 1–11. https://doi.org/10.1109/63.208493

Bolte, S., Froehleke, N., & Boecker, J. (2016). Isolated On-Board DC-DC Converter for Power Distribution Systems in Electric Vehicles. In *PCIM Europe 2016; International Exhibition and Conference for Power Electronics, Intelligent Motion, Renewable Energy and Energy Management* (pp. 1–7). Nuremberg, Germany: VDE.

Chau, K. ., & Wong, Y. . (2002). Overview of power management in hybrid electric vehicles. *Energy Conversion and Management*, *43*, 1953–1968. https://doi.org/10.1016/S0196-8904(01)00148-0

Dearborn, S. (2005). Charging Li-ion Batteries. *Power Electronics Technology*, (April), 40–49.

Erb, D. C., Onar, O. C., & Khaligh, A. (2010). Bi-directional charging topologies for plug-in hybrid electric vehicles. In *Conference Proceedings - IEEE Applied Power Electronics Conference and Exposition - APEC* (pp. 2066–2072). https://doi.org/10.1109/APEC.2010.5433520

Garcia, O., Flores, L. a., Oliver, J. a., Cobos, J. a., & de la Pena, J. (2005). Bi-directional DC/DC Converter for Hybrid Vehicles. In *IEEE 36th Conference on Power Electronics Specialists, 2005.* (pp. 1881–1886). https://doi.org/10.1109/PESC.2005.1581888

Kang, Y. G., Upadhyay, A. K., & Stephens, D. L. (1991). Analysis and Design of a Half-Bridge Parallel Resonant Converter Operating Above Resonance. *IEEE Transactions on Industry Applications*, *27*(2), 386–395. https://doi.org/10.1109/28.73630

Kazimierczuk, M. K. (2012). *Pulse-Width Modulated DC-DC Power Converters*. *Pulse-Width Modulated DC-DC Power Converters*. https://doi.org/10.1002/9780470694640

Kisacikoglu, M. C., Kesler, M., & Tolbert, L. M. (2015). Single-phase on-board bidirectional PEV charger for V2G reactive power operation. *IEEE Transactions on Smart Grid*, *6*(2), 767–775. https://doi.org/10.1109/TSG.2014.2360685

Kisacikoglu, M. C., Ozpineci, B., & Tolbert, L. M. (2010). Examination of a PHEV bidirectional charger system for V2G reactive power compensation. In *Conference Proceedings - IEEE Applied Power Electronics Conference and Exposition - APEC* (pp. 458–465). https://doi.org/10.1109/APEC.2010.5433629

Kisacikoglu, M. C., Ozpineci, B., & Tolbert, L. M. (2011). Reactive power operation analysis of a single-phase EV/PHEV bidirectional battery charger. In *8th International Conference on Power Electronics - ECCE Asia* (pp. 585–592). IEEE. https://doi.org/10.1109/ICPE.2011.5944614

Kisacikoglu, M. C., Ozpineci, B., & Tolbert, L. M. (2013). EV/PHEV bidirectional charger assessment for V2G reactive power operation. *IEEE Transactions on Power Electronics*, *28*(12), 5717–5727. https://doi.org/10.1109/TPEL.2013.2251007

Liu, K.-H., Oruganti, R., & Lee, F. C. (1985). Resonant switches - Topologies and characteristics. In *1985 IEEE Power Electronics Specialists Conference* (pp. 106–116). https://doi.org/10.1109/PESC.1985.7070935

Maniktala, S. (2012). *Switching power supplies A-Z* (Second edi). Oxford: Newnes.

Mohan, N., Underland, T., & Robbins, W. (2003). *Power Electronics: Converters, Applications, And Design* (Third). Hoboken, NJ: John Wiley & Son, Inc.

Rani, S. M., Samantaray, J., & Dash, S. S. (2013). Analysis of Full Bridge Series Parallel Resonant Converter for Battery Chargers. In *Advanced Materials Research* (pp. 388–391). Trans Tech Publications.

Severns, R. P. (1992). Topologies for three-element resonant converters. *IEEE Transactions on Power Electronics*, *7*(1), 89–98. https://doi.org/10.1109/63.124581

Tan, X., & Ruan, X. (2016). Equivalence Relations of Resonant Tanks: A New Perspective for Selection and Design of Resonant Converters. *IEEE Transactions on Industrial Electronics*, *63*(4), 2111–2123. https://doi.org/10.1109/TIE.2015.2506151

Tv, P. D. P., & Mosfets, P. (2007). Application note LLC resonant half-bridge converter design guideline. *ReVision*, (October), 1–32.

Wan, H. (2012). *High Efficiency DC-DC Converter for EV Battery Charger Using Hybrid Resonant and PWM Technique*. Virginia Polytechnic Institute and State University.

Wang, H., Dusmez, S., & Khaligh, A. (2014). A novel approach to design EV battery chargers using SEPIC PFC stage and optimal operating point tracking technique for LLC converter. In *2014 IEEE Applied Power Electronics Conference and Exposition - APEC 2014* (pp. 1683–1689). IEEE. https://doi.org/10.1109/APEC.2014.6803532

Yang, E. X., Lee, F. C., & Jovanovic, M. M. (1992). Small-signal modeling of LCC resonant converter. In *Power Electronics Specialists Conference, 1992. PESC '92 Record., 23rd Annual IEEE* (pp. 941–948 vol.2). https://doi.org/10.1109/PESC.1992.254782

Yilmaz, M., & Krein, P. T. (2013). Review of battery charger topologies, charging power levels, and infrastructure for plug-in electric and hybrid vehicles. *IEEE Transactions on Power Electronics*. https://doi.org/10.1109/TPEL.2012.2212917